REVIEW

View Article Online
View Journal | View Issue

Single-atom and cluster catalysts for thermocatalytic ammonia synthesis at mild conditions

Xuanbei Peng,†[ab] Mingyuan Zhang,†[a] Tianhua Zhang,†[a] Yanliang Zhou,*[ab] Jun Ni,[a] Xiuyun Wang [iD] *[ab] and Lilong Jiang [iD] *[ab]

Ammonia (NH_3) is closely related to the fields of food and energy that humans depend on. The exploitation of advanced catalysts for NH_3 synthesis has been a research hotspot for more than one hundred years. Previous studies have shown that the Ru B_5 sites (step sites on the Ru (0001) surface uniquely arranged with five Ru atoms) and Fe C_7 sites (iron atoms with seven nearest neighbors) over nanoparticle catalysts are highly reactive for N_2-to-NH_3 conversion. In recent years, single-atom and cluster catalysts, where the B_5 sites and C_7 sites are absent, have emerged as promising catalysts for efficient NH_3 synthesis. In this review, we focus on the recent advances in single-atom and cluster catalysts, including single-atom catalysts (SACs), single-cluster catalysts (SCCs), and bimetallic-cluster catalysts (BCCs), for thermocatalytic NH_3 synthesis at mild conditions. In addition, we discussed and summarized the unique structural properties and reaction performance as well as reaction mechanisms over single-atom and cluster catalysts in comparison with traditional nanoparticle catalysts. Finally, the challenges and prospects in the rational design of efficient single-atom and cluster catalysts for NH_3 synthesis were provided.

1. Introduction

The excessive consumption of conventional fossil fuels in the modern industrial world has led to the increasing pressure of energy crisis and environmental pollution on human society.[1] To achieve the goal of zero carbon emissions in 2060, there is an urgent need to develop and utilize renewable and environmentally friendly energy sources so as to move towards a low-carbon society and economy. However, sustainable and renewable energy face a compatibility issue with the current large-scale and established energy infrastructure because of their intrinsic intermittence and fluctuation. The application of energy storage carrier is an efficient route to solve the utilization of renewable energy. It is general knowledge that hydrogen serves as a clean energy. Recently, with the green generation of electricity using renewable sources (such as hydro, wind, solar and tidal), it becomes economically acceptable to use the H_2 produced by water electrolysis. However, high pressure transportation (∼20 MPa) currently hinders its large-scale application.[2] Therefore, it is important to develop hydrogen production, storage and transportation systems that allow hydrogen to be distributed and utilized in a safe manner.[3]

Ammonia (NH_3) is an important chemical product with a wide range of applications in modern society, such as the production of fertilizers, pharmaceuticals, explosives, and other nitrogen-containing compounds.[4-6] In addition, NH_3 is also a promising carbon-free energy storage carrier for storing intermittent renewable energy sources.[7,8] Compared to liquid hydrogen and other organic liquid hydrogen energy carriers (such as toluene and cyclohexane),[3] NH_3 is preferred as an energy carrier due to its high energy density (4.32 kW h L^{-1}), high gravimetric (17.6 wt%) and volumetric (121 kg m^{-3}) hydrogen densities, and ease of liquefaction under mild conditions.[9-12] Moreover, the storage and transportation systems of liquid NH_3 are mature and safe.[9] Currently, the industrial production of NH_3 is mainly through the Haber–Bosch (HB) process using Fe-based catalysts at high temperatures (490–510 °C) and high pressures (15–30 MPa).[13,14] To meet the global demand for NH_3, approximately 200 million tons of NH_3 are produced annually using the HB process, which consumes about 1–2% of the global annual energy supply and also results in significant carbon dioxide emissions.[5,15-17] With the maturity of water electrolysis technology driven by renewable electric power, the carbon emission problem in NH_3 synthesis will be solved properly by coupling water electrolysis for H_2 production technology with the electrolysis-driven HB (eHB) process.[18-20] The present bottleneck is that NH_3 cannot be synthesized under mild conditions, resulting in mismatch with the pressure of the electrolysis system employed for H_2 production (<5 MPa, mostly in the range of 1.0–3.2 MPa).

[a]National Engineering Research Center of Chemical Fertilizer Catalyst, Fuzhou University, Fuzhou, Fujian, 350002, China. E-mail: zhouyl@fzu.edu.cn; xywangfzu@163.com; jll@fzu.edu.cn

[b]Qingyuan Innovat Lab, Quanzhou, Fujian, 362801, China

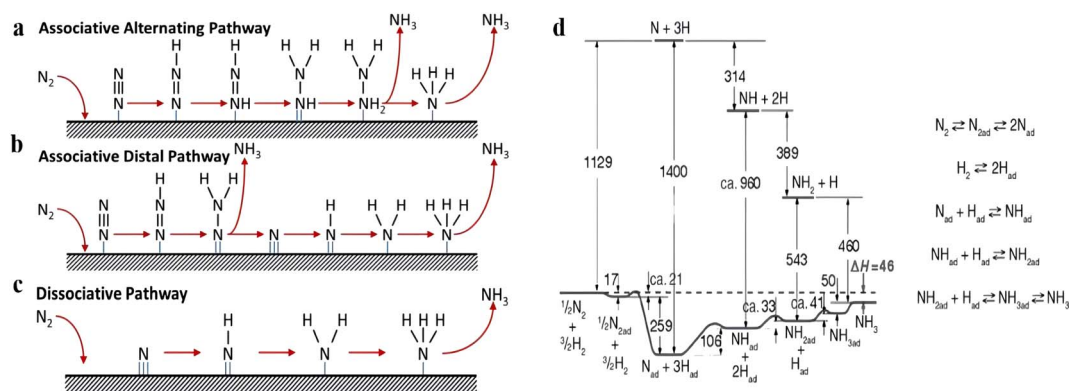† These authors contributed equally to this work.

Fig. 1 (a) Associative alternating pathway, (b) associative distal pathway, and (c) dissociative pathway for NH_3 synthesis on heterogeneous catalysts.[21] (d) Mechanism and potential energy diagram of NH_3 synthesis on the iron surface.[22]

Accordingly, the design and development of efficient NH_3 synthesis catalysts under mild conditions are keenly needed.

The main bottleneck for the synthesis of NH_3 is the activation of the inert N_2, primarily due to its high N≡N triple bond energy (941 kJ mol^{-1}), lack of a permanent dipole, a large HOMO–LOMO gap (10.8 eV) and a high ionization energy (15.58 eV),[23,24] making it difficult to activate under mild conditions. At present, the activation route of N_2 has been widely studied, which involves
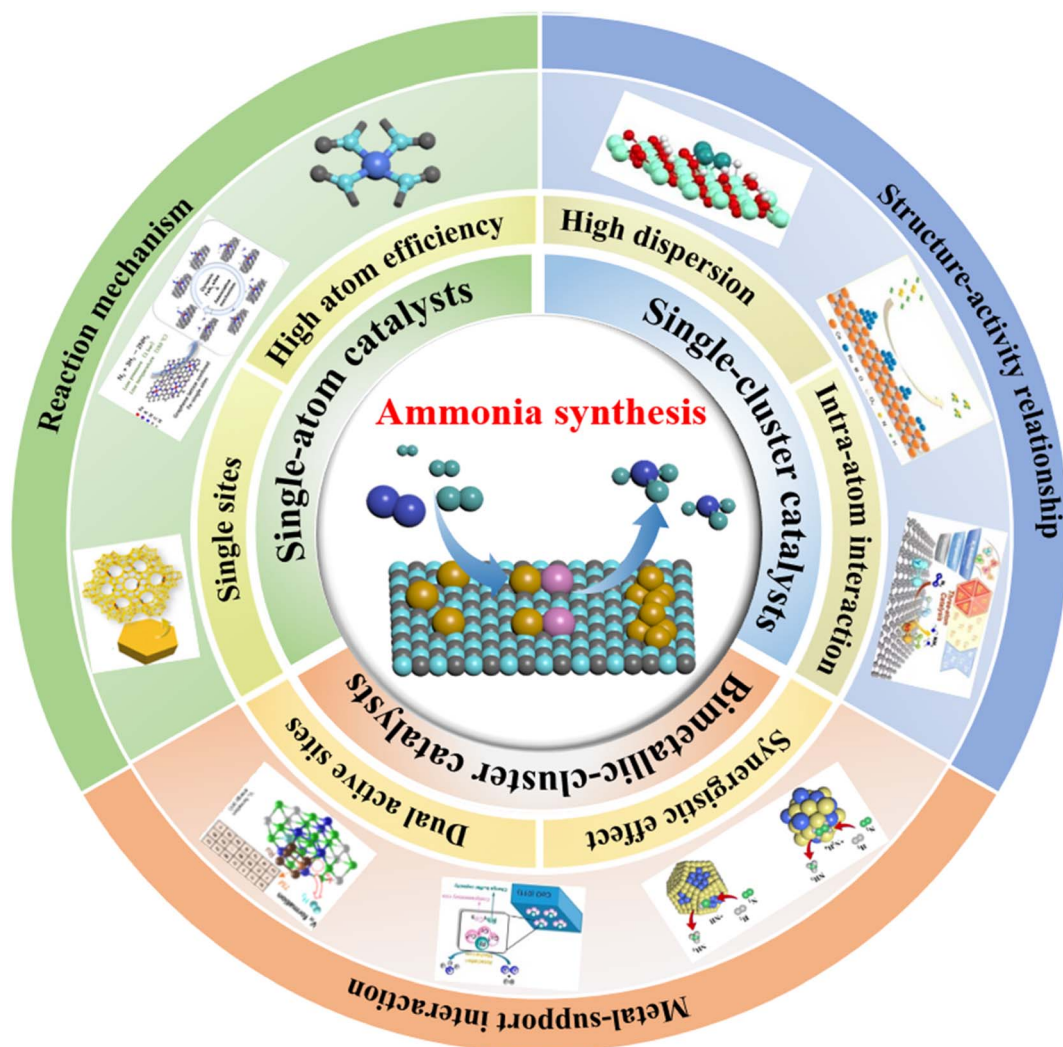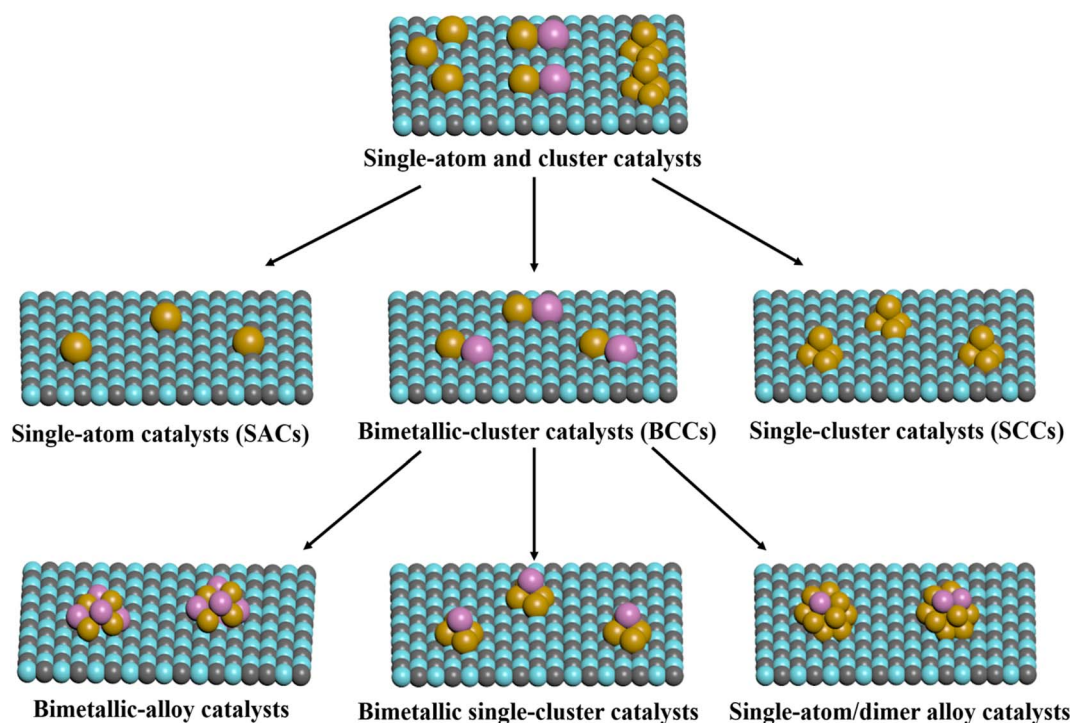

Scheme 1 Schematic for single-atom and cluster catalysts for thermocatalytic NH_3 synthesis.

either the associative or dissociative route. In both photocatalytic and electrocatalytic synthesis of NH_3, the mild reaction conditions cannot realize the direct dissociation of the $N\equiv N$ triple bond while enabling the hydrogenation of N_2 *via* an associative mechanism with the assistance of an external field (Fig. 1a and b).[25–27] For alternate hydrogenation, the two N atoms are hydrogenated by protons to form *NH–NH and *NH_2–NH_2 species, whereas for distal hydrogenation, protons are bonded to one N atom to form the *N–NH_2 and *N–NH_3 species. Comparatively, due to the existence of certain temperature and pressure in the thermocatalytic NH_3 synthesis, N_2 is more likely to form NH_3 *via* the dissociative mechanism, whereby the adsorbed N_2 dissociates directly into the adsorbed N atoms (2N), followed by stepwise hydrogenation to form NH_3 (Fig. 1c). As early as 1934, Emmett and Brunauer speculated that the formation rate of NH_3 should be approximately equal to the dissociation rate of N_2 on the surface of the iron-based catalysts.[28] Subsequently, Ertl and his colleagues further confirmed this viewpoint through a series of surface characterization techniques on Fe-based catalysts, and they revealed the process of NH_3 synthesis *via* a dissociative mechanism (Fig. 1d).[22,29,30] Concurrently, the dissociative adsorption of N_2 is generally considered as the rate-determining step (RDS) for NH_3 synthesis, which is closely related to unique active sites on the transition metal surface, such as the C_7 sites of Fe.[31,32] The so-called C_7 active sites mean seven adjacent Fe atoms on the surface of an Fe single crystal.[33,34] Somorjai and Strongin *et al.* studied the high-pressure NH_3 synthesis on different crystal faces of Fe single crystal and found that the NH_3 synthesis activity presented in the following order: Fe (111) > Fe (211) > Fe (100) > Fe (210) > Fe (110).[31,34–37] The catalytic activity of Fe (111)

and (100) surfaces was *ca.* 418 and 25-fold higher than that of tightly packed Fe (110) surfaces, respectively, indicating that the NH_3 synthesis over Fe catalysts is a structure-sensitive reaction. The high activity of NH_3 synthesis at Fe (111) was mainly attributed to the presence of a large number of C_7 active sites, which facilitated the significant weakening of the π bond in $N\equiv N$ and promoted its dissociation.[31] The dissociative mechanism on the Fe (111) surface was also further verified by Nørskov *et al.* using density functional theory (DFT) calculations.[38]

Compared with Fe-based catalysts, the NH_3 synthesis over Ru is considered to be more structurally sensitive through DFT calculations and extensive studies on Ru single crystals.[39–41] Moreover, N_2 dissociation on Ru (0001) surface was considered to be entirely dominated by the B_5 sites,[39,40] which exposed a three-fold hollow site with a bridge site in close proximity to assure two nitrogen atoms of N_2 not bonding to the same Ru atom. The concentration of the B_5 sites strongly depends on the size and shape of Ru nanoparticles (Ru NPs), with the highest concentration of B_5 active sites in 1.8–2.5 nm Ru NPs, whereas almost no B_5 active sites exist when the particle size of Ru NPs is less than 1.8 nm.[33,42,43] In the past few decades, numerous efforts have been made to develop various high-performance transition metal catalysts to lower the dissociation energy of N_2, but only a few novel catalysts have been able to shift the bottleneck from slow N_2 dissociation to the formation of N–H_x (x = 1–3).[44–46] In recent years, theoretical and experimental studies have demonstrated that in thermocatalytic NH_3 synthesis, when the particle size of metal nanoparticles is reduced to the sub-nanometer clusters, atomic clusters or even single atom level, in which effective sites for N_2 dissociation cannot be formed; N_2 is

Scheme 2 Schematic diagram of classification over single-atom and cluster catalysts.

inclined to be activated *via* an associative mechanism for NH_3 synthesis.[47–49] It has been shown that controlling active metal in the form of subnano clusters or single atoms is an efficient method to improve their catalytic activity and utilization.[49–51] Therefore, transition metal catalysts at the nanoscale, sub-nanoscale, especially at the atomic level, have received widespread attention in the field of NH_3 synthesis in recent years.

In this review, the recent progress in single-atom and cluster catalysts, including SACs, SCCs, and BCCs, for thermocatalytic NH_3 synthesis is presented for both the theoretical development and experimental practice (Schemes 1 and 2). The unique properties and reaction mechanisms over single-atom and cluster catalysts compared with traditional nanoparticle catalysts are discussed and summarized. In addition, we also discuss the current challenges and future prospects of the design of single-atom and cluster catalysts for NH_3 synthesis under mild conditions. The purpose of this review is to deepen the fundamental understanding and give guidance for the rational design of advanced catalysts for NH_3 synthesis.

2. SACs for NH_3 synthesis

In recent years, SACs have garnered widespread attention in the field of heterogeneous catalysis for their maximum atom efficiency and excellent catalytic performance, mainly due to the significant advantages of SACs in terms of activity, selectivity, and tunable interactions between metal atoms and supports.[52–54] Currently, there are various synthesis methods for SACs, such as high-temperature pyrolysis,[55] co-precipitation,[56] one-pot synthesis,[57] and atomic layer deposition (ALD).[58]

However, isolated metal atoms with high surface free energy are prone to migrate and aggregate under reaction conditions. Therefore, various supports including carbon materials, nitrogen-doped carbon-based materials, metal oxides, and zeolites are typically employed in the preparation process to disperse and stabilize metal atoms.[59–61] Besides, according to the property of active metal in SACs for NH_3 synthesis, it can be simply classified as noble metal SACs and non-noble metal SACs.

2.1 Noble metal SACs

Noble metals, which are active for NH_3 synthesis, are mainly represented by Os and Ru. Therein, the research and application of Os is limited because of its scarcity, while Ru-based catalysts are regarded as the second-generation catalysts for NH_3 synthesis. Due to the high cost of the noble metal Ru, developing Ru SACs can maximize its atomic efficiency while providing well-defined single-atom sites for mechanism study.[62] Qiu *et al.* prepared pure siliceous zeolite-supported Ru single-atom catalyst (Ru SAs/S-1) using hydrothermal and vacuum decomposition methods (Fig. 2a).[63] At 523–648 K and 0.1 MPa, the NH_3 synthesis rate of Ru SAs/S-1 was higher than that of the traditional Cs–Ru/MgO catalyst with similar Ru content (Fig. 2b), indicating that the single Ru active site exhibited excellent catalytic performance, which was associated with its distinct N_2 activation pathway. The N_2 reaction order of Ru SAs/S-1 was determined to be 0.15, which was much lower than that of traditional Ru-based catalysts (close to unity), indicating that the dissociation of N_2 was no longer the rate-determining step.[64] Moreover, the H_2 reaction order over Ru SAs/S-1 is a positive

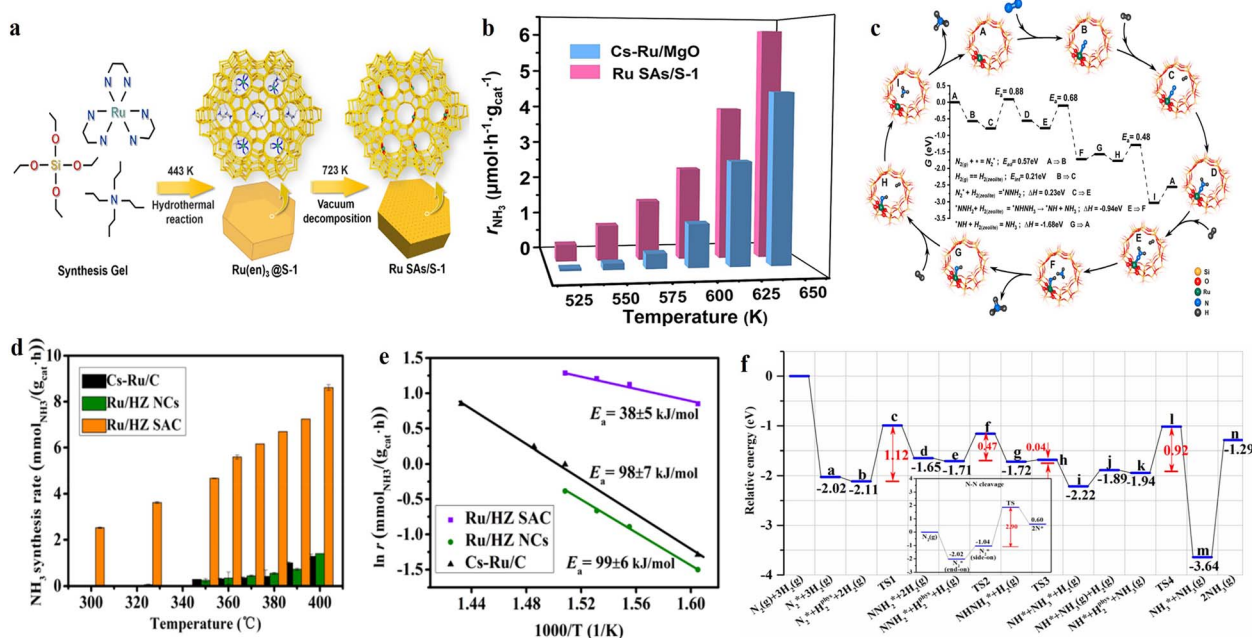

Fig. 2 (a) Synthesis procedure of Ru SAs/S-1. (b) Temperature dependence of NH_3 synthesis rate over Ru SAs/S-1 and Cs−Ru/MgO varying from 523 to 648 K. (c) DFT calculation of NH_3 synthesis reaction pathway over the Ru SAs/S-1 catalyst.[63] (d) NH_3 synthesis rate and (e) Arrhenius plots of Ru/HZ SAC and Ru/HZ NCs catalysts as well as the Cs−Ru/C reference. (f) Potential energy diagrams for NH_3 synthesis on Ru/HZ SAC *via* the formation of NNH_2* as intermediates.[65]

value (0.36), which was different from the generally negative value for conventional Ru catalysts. DFT calculations indicated that N_2 molecules can be linearly adsorbed in the exposed Ru single-atom active sites and reacted with H_2 molecules physically adsorbed in the zeolite channels to form NH_3 *via* a distal pathway of associative mechanism (Fig. 2c). Similarly, Li *et al.* employed HZSM-5 (HZ) zeolite with a rich microporous structure to serve as an anchoring site for stabilizing Ru single atoms (Ru/HZ SAC) by integrating a microwave single mode and ion exchange method.[65] Ru/HZ SAC with 0.2 wt% Ru exhibited excellent NH_3 synthesis rate of 4.67 $mmol_{NH_3}$ g_{cat}^{-1} h^{-1} at 350 °C and 1 MPa, which was approximately 20-fold higher than that of Ru/HZ NCs (Fig. 2d). Moreover, the apparent activation energy for NH_3 synthesis over Ru/HZ SAC (38 kJ mol^{-1}) (Fig. 2e) was significantly less than that of the conventional Ru-based catalysts (80–130 kJ mol^{-1}),[66,67] indicating the different reaction mechanism over the Ru/HZ SAC catalyst for NH_3 synthesis. DFT calculations indicated that the direct dissociation of N_2 into 2N on a single Ru site required a high energy barrier of 2.90 eV, while the hydrogenation *via* a distal pathway of associative mechanism to form $*NNH_2$ required only 1.12 eV (Fig. 2f), indicating that the dissociation adsorption pathway on Ru SACs was not favorable for NH_3 synthesis.

2.2 Non-noble metal SACs

Compared with noble metal Ru-based catalysts, the development of non-noble metal single-atom catalysts are more attractive for industrial applications. Notably, carbon materials or N-doped carbon materials have been frequently reported as excellent supports for SACs due to their large specific surface area, tunable electronic structure, and electron transfer capability.[68] Wang *et al.* reported the N-doped carbon-supported Co SACs (Co–N–C) for NH_3 synthesis under mild conditions.[48] At 350 °C and 1 MPa, the NH_3 synthesis rate of the Co–N–C catalyst was 4.34 $mmol_{NH_3}$ g_{cat}^{-1} h^{-1}, which was 11- and 17-fold higher than that of Co/C and N–C, respectively (Fig. 3a). The outstanding performance of Co–N–C for NH_3 synthesis was attributed to the synergistic effect of dynamic and steady-state dual-active sites. The stable $Co_1–N_{3.5}$ active site formed by the coordination of Co with the pyrrolic N in the support facilitated the activation of N_2 *via* the alternate pathway of associative mechanism, resulting in the stepwise hydrogenation to form $*HNNH$, $*NH–NH_3$, and $*NH_2–NH_4$ species, followed by the cleavage of the N–N bond in $*NH_2–NH_4$ species to release NH_3 (Fig. 3b). Moreover, the pyridine N species, which interacted less strongly with Co, can react with adsorbed H_2 to form NH_3 *via* a chemical looping pathway (Fig. 3c). To investigate the influence of different coordination environments
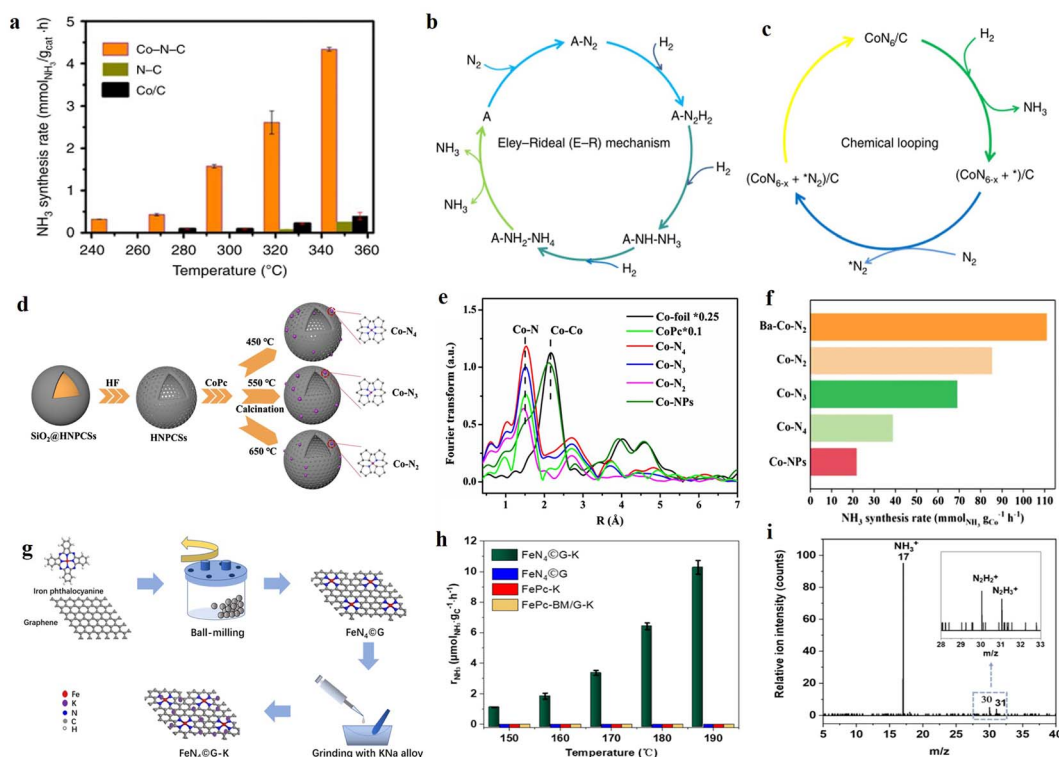

Fig. 3 (a) NH_3 synthesis rate for Co–N–C, Co/C, and N–C under 1 MPa. (b) NH_3 synthesis pathway on single Co sites in the form of steady-state $Co_1–N_{3.5}$ (A represents the active sites); (c) NH_3 production on dynamic cyclic sites *via* the chemical-looping pathway (x is in the range of $0 < x \leq$ 1.5 and V_N* represents an anionic nitrogen vacancy).[48] (d) Schematic diagram of the preparation process of Co–N_x with different CNs. (e) Co K-edge EXAFS spectra of Co–N_x catalysts. (f) NH_3 synthesis rate over the as-synthesized Co–N_x catalysts at 1 MPa and 300 °C. (g) Scheme for the preparation of the graphene lattice-confined Fe-single-site catalyst $FeN_4©G-K$. (h) Production rates of $FeN_4©G-K$, $FeN_4©G$, $FePc-K$, and $FePc-BM/G-K$ as a function of reaction temperature at 0.1 MPa. (i) The effluents monitored by in NH_3 synthesis over $FeN_4©G-K$ at 180 °C, 0.1 MPa, and WHSV of 30 L g_c^{-1} h^{-1}.[71]

in SACs on NH_3 synthesis performance, Zhou *et al.* prepared atomically dispersed Co-based catalysts with different Co–N coordination numbers by varying the pyrolysis temperatures.[69] With the increase in the pyrolysis temperature, the coordination number of Co–N decreased gradually. Co SACs with Co–N_4, Co–N_3, and Co–N_2 coordination structures were obtained at 450, 550 and 650 °C, respectively (Fig. 3d and e). Compared with Co–N_4 and Co–N_3 catalysts, the Co–N_2 catalyst with the lowest coordination number exhibited the best catalytic activity, with an NH_3 synthesis rate of 85.3 $mmol_{NH_3}\ g_{Co}^{-1}\ h^{-1}$ at 300 °C and 1 MPa (Fig. 3f). Various characterizations and DFT calculations elucidated that Co SAC with low coordination number could generate more unoccupied Co 3d charges and tetrahedral cobalt(II) sites, which can promote the electron transfer for N_2 activation and the desorption N-containing intermediate species, respectively, thus resulting in a high NH_3 synthesis rate. Similarly, Li *et al.* studied Co SACs with different Co–N coordination numbers and also showed that Co–N_2 catalysts with two coordination N atoms exhibited the best NH_3 synthesis performance,[70] which was attributed to the fact that Co SACs with low Co–N coordination were conducive to N_2 adsorption and activation.

In addition to Co-based single-atom catalysts, Fe- or Mo-based single-atom catalysts also exhibited excellent NH_3 synthesis performance. Chen *et al.* successfully confined the FeN_4 structure to the lattice of graphene by co-milling FePc and graphene at 450 rpm for 20 h (Fig. 3g).[71] The FeN_4©G-K catalyst with 24.5 wt% K showed an excellent catalytic activity under mild conditions, with NH_3 synthesis rates of 1.1 and 10.3 $\mu mol_{NH_3}\ g_c^{-1}\ h^{-1}$ at 150 °C and 190 °C, respectively (Fig. 3h). This study results revealed that the effective active site of the FeN_4©G-K catalyst for N_2 activation was FeN_3, and NH_3 was formed by gradual hydrogenation *via* an associative mechanism. Interestingly, the real-time detection of $N_2H_2^+$ and $N_2H_3^+$ intermediate species by time-of-flight mass spectrometer (TOF-MS) further experimentally verified the synthesis of NH_3 by associative mechanism at the single atomic active site (Fig. 3i). Azofra *et al.* fabricated single Mo active sites confined in Si-based materials and applied it in the synthesis of NH_3.[72] At 400 °C and atmospheric pressure, the NH_3 synthesis rate reached 1.3 $mmol\ g_{Mo}^{-1}\ h^{-1}$. Theoretical calculations indicated that N_2 spontaneously adsorbed and was activated on the $[(\equiv Si–O–)MoH_3]$ site *via* an associative mechanism, where the rate-determining step is the further hydrogenation of the adsorbed *$NHNH_2$ to form NH_3.

In summary, SACs possess a unique geometric and electronic structure as well as complete metal dispersion compared with nanoparticle catalysts. The single-atom sites over SACs cannot realize the direct dissociation of N_2 while enabling N_2 activation *via* an associative route for NH_3 synthesis. The distinct reaction mechanism on SACs in comparison with nanoparticle catalysts is conducive to realizing higher NH_3 synthesis rate at mild conditions. Nevertheless, the disadvantages of SACs for NH_3 synthesis are also obvious. On the one hand, due to the high surface free energy, the single atoms are easy to migrate and agglomerate. Moreover, the metal loading of SACs is generally low, which limits the catalytic activity of NH_3 synthesis. On the other hand, it is difficult for a single-atom active site to activate both N_2 and H_2 molecules at the

same time, which may result in hydrogen poisoning phenomena, such as the observation of negative H_2 reaction order in Ru_1/CeO_2.[73] Therefore, developing high-loading SACs or combining single atoms with other active centers are effective strategies to further improve the NH_3 synthesis performance.

3. SCCs for NH_3 synthesis

Unlike SACs where single atoms are highly dispersed on the support in isolation, a number of atoms assembled in the form of individual clusters can form single-cluster catalysts, which results in unique geometric and electronic structure. The cluster catalysts can not only provide multiple metal atoms as catalytic sites but also possess high metal dispersion. The single-cluster catalyst can be simply classified as noble metal SCCs and non-noble metal SCCs.

3.1 Noble metal SCCs

It is well known that NH_3 synthesis is a size-sensitive reaction, where the size of Ru has a significant impact on the activity of NH_3 synthesis. According to DFT calculation based on the model of Wulff construction, when the particle size was between 1.8 and 2.5 nm, the number of Ru B_5 sites was enriched, which was conducive to the adsorption and dissociation of N_2.[33] Jacobsen *et al.* also indicated that the optimal Ru particle size was approximately 2 nm, which can maximize the proportion of B_5 sites to improve NH_3 synthesis performance. When the size of Ru particle was less than 2 nm, the proportion of corner sites increased along with the decreased in the number of B_5 sites. Therefore, previous research predicted that the small Ru clusters in the absence of B_5 sites were supposed to be inactive in NH_3 synthesis.[74]

Nevertheless, recent studies have shown that the activity of NH_3 synthesis increases with the decrease in Ru particle size. For instance, Zhou *et al.* synthesized a series of $Ru/BaCeO_3$ catalysts with various Ru particle sizes (1.1–3.0 nm) using size-controlled Ru colloids as precursors.[75] The experimental results showed that the NH_3 synthesis rate significantly increased as the Ru particle size decreased from 3.0 nm to 1.1 nm. At 400 °C and 1 MPa, the $TOF_{Ru\ total}$ of Ru1.1/$BaCeO_3$ can reach up to 0.124 s^{-1}, which was about 6-fold higher that of Ru3.0/$BaCeO_3$ (Fig. 4a). It was revealed that the small Ru clusters were conducive to the formation of Ce^{3+} and O_v species in $BaCeO_3$, which promoted the electron transfer from Ru metal to N_2, thereby accelerating the dissociation of N_2. In addition, the small Ru clusters enhanced hydrogen spillover from Ru to $BaCeO_3$ support to alleviate hydrogen poisoning, resulting in efficient NH_3 synthesis. Similarly, Peng *et al.* used N-doped carbon as a carrier and prepared a series of Ru catalysts with sizes ranging from 1.4 to 5.0 nm using colloidal Ru deposition method.[19] The study found that the TOF of 5 nm Ru NPs was 2.53 × $10^{-2}\ s^{-1}$. When the particle size decreased from 5.0 nm to 1.4 nm, the TOF increased to 5.23 × $10^{-2}\ s^{-1}$, mainly due to the increase in the corner sites of the catalyst (Fig. 4b), which was beneficial for reducing the work function and promoting N_2 activation. These results unravel the size-dependent effect of
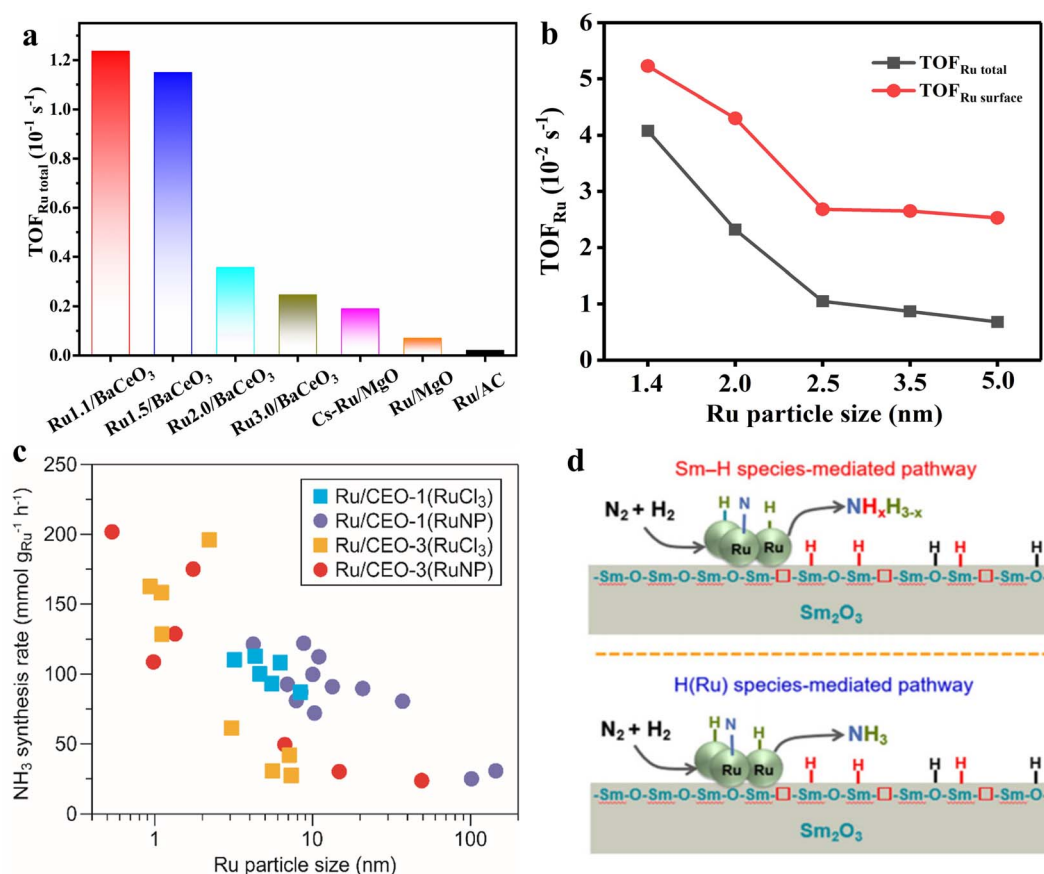
Fig. 4 (a) $TOF_{Ru\ total}$ of the Ru_xBeCeO_3 catalysts at 400 °C and 1 MPa.[75] (b) TOF_{Ru} of Ru NCs at 400 °C and 1 MPa.[19] (c) NH_3 synthesis rate of Ru/CEO-1 and Ru/CEO-3 catalysts at 400 °C and 0.1 MPa as a function of the mean Ru particle size.[80] (d) Schematic illustration of chemisorbed H(Ru) species-mediated and Sm–H species-mediated reaction pathways on the Ru/Sm_2O_3 catalyst. Color code for different kinds of H species: H(Ru), Sm–H and O–H species are shown in blue, red and black, respectively.[81,82]

Ru-based catalysts and highlight the superior activity of Ru cluster catalysts in NH_3 synthesis.

In recent years, an increasing number of Ru cluster catalysts have been reported to exhibit high NH_3 synthesis performance. Li *et al.* found that the activity of Ru/MgO-MIL with small Ru clusters (1.0 nm) in NH_3 synthesis was approximately 19 times that of traditional 2–4 nm Ru/MgO catalyst and 7.7 times that of Ru@MIL-101.[76] The superior mass activity was largely due to the efficient utilization of Ru atomic clusters. Meanwhile, the authors believed that the theoretical model of Ru particles was based on the Wulff construction, while under realistic conditions, small clusters might deviate from the ideal thermodynamic model and generate B_5 sites on the surface.[77,78] Feng *et al.* synthesized CeO_2 nanorods-supported subnano Ru clusters for NH_3 synthesis at mild conditions.[79] The Ru clusters/CeO_2 exhibited a much higher activity in NH_3 synthesis than the Ru nanoparticle counterpart. It was revealed that the sub-nanometer Ru clusters species facilitated the activation and dissociation of H_2 and N_2 molecules, mainly responsible for its intrinsic activity in NH_3 synthesis. Similarly, Hirabayashi *et al.* also found that the Ru small clusters over Ru/CeO_2 exhibited a superior NH_3 synthesis performance (Fig. 4c).[80] Furthermore, the Sm_2O_3-supported sub-nanometer Ru cluster catalyst was

developed and exhibited superior NH_3 synthesis performance. Mechanistic studies and theoretical calculations showed that for the activated Ru/Sm_2O_3, a large amount of surface Sm–H species could be generated on Sm_2O_3 (Fig. 4d). The Sm–H species not only can cooperate with Ru clusters to reduce the energy barrier of nitrogen dissociation but also can directly participate in the formation of NH_3 on Ru clusters.[81,82]

Theoretical calculations in recent years also support the idea that cluster catalysts promote NH_3 synthesis more effectively. Taking the Ru_3 clusters as an example, Wang *et al.* investigated the Ru_3 single clusters anchored on the defective g-C_3N_4 nanosheet (Ru_3/Nv-g-C_3N_4) for NH_3 synthesis based on DFT calculations and microscopic kinetic simulations.[83] Under the industrial reaction conditions of NH_3 synthesis at 673 K and 100 bar, the TOF of Ru_3/Nv-g-C_3N_4 is 5.8 times that of the Ru (0001) step surface. DFT calculations revealed that the reaction proceeded parallelly on Ru_3/Nv-g-C_3N_4 through both dissociative and alternative associative mechanisms. With increasing temperatures or decreasing pressures, the dissociative mechanism gradually prevailed and the associative mechanism receded (Fig. 5a and b). Furthermore, Cheng used Ru_{19} clusters as an example to calculate the free energy distribution of a typical catalytic reaction[84] based on *ab initio* molecular
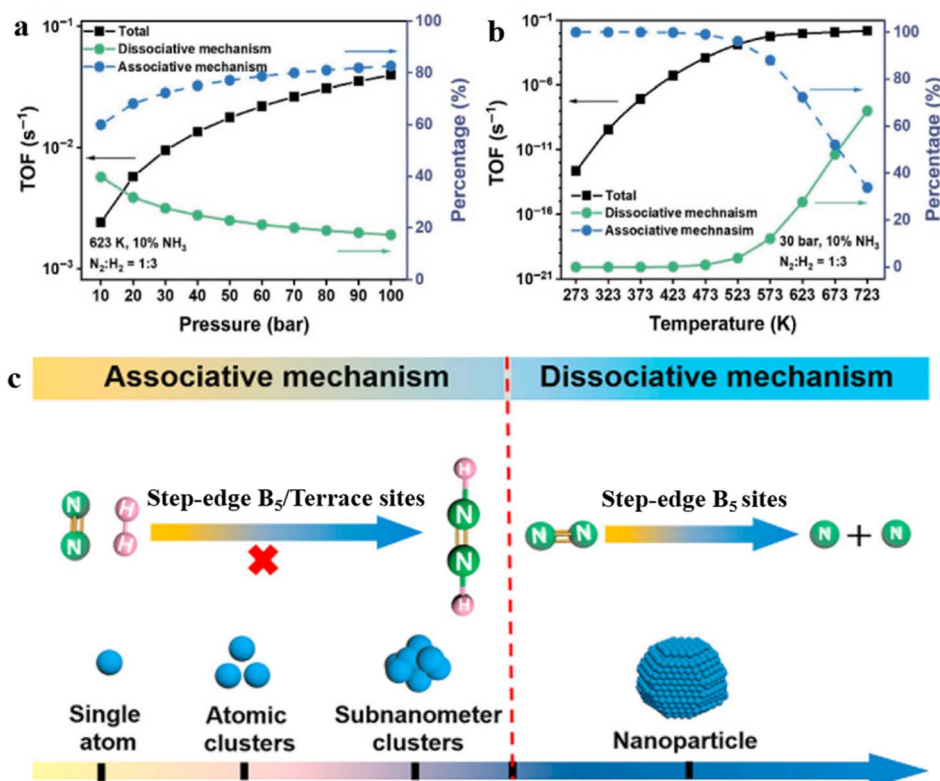
Fig. 5 TOFs and contributions from dissociative and associative mechanisms as functions of (a) pressure under constant temperature of 623 K, (b) temperature under constant pressure of 30 bar.[83] (c) NH_3 synthesis pathway over Ru catalysts with different sizes.[49]

dynamics (AIMD) and free energy methods. It was found that the reaction free energies (DrG) and barrier (DGa) of the Ru_{19} clusters were quite different from those obtained from static geometric optimization methods, indicating that the dynamic fluctuations of clusters configurations significantly affected the reaction free energy and potential barrier. Notably, the phase transition of sub-nanometer clusters can accelerate the N_2 activation due to the reduction of reaction free energy and enabling NH_3 synthesis at low temperatures.

Due to the absence of Ru B_5 sites over Ru clusters, the reaction mechanism over Ru clusters may be different from Ru nanoparticle catalysts. Zhou *et al.* reported the design of sub-nanocluster Ru clusters (0.8 nm) anchored on hollow N-doped carbon spheres (Ru-SNCs) catalysts.[85] Under 400 °C and 3 MPa conditions, the TOF_{Ru} of 0.5Ru-SNC (0.067 s^{-1}) was 3.5 times higher than that of the 1.2Ru-NPs catalyst (0.019 s^{-1}). The UV-vis and *in situ* infrared experiments showed that the N_2H_4 species was the main intermediate for NH_3 synthesis on the Ru-SNCs catalyst. It demonstrated that the Ru–SNCs catalyst can follow an associative route for N_2 activation, which circumvented the direct dissociation of N_2 and resulted in highly efficient NH_3 synthesis at mild conditions. Furthermore, Li *et al.* synthesized a series of Ru catalysts with Ru sizes ranging from single atoms, atomic clusters, sub-nanometric clusters, to nanoparticles.[49] Researches showed that with the size decrease of Ru nanoparticle to sub-nanometric and atomic level, the activation pathway of N_2 changed from dissociative mechanism

to associative mechanism (Fig. 5c). At the sub-nanometric level, the enhanced intra-cluster interaction of atomic clusters up-shifted the Ru d-band center toward the Fermi level, thus significantly promoting N_2 activation *via* the associative mechanism with extremely small reaction energy barriers. In addition, the synergistic effect of single atom and cluster for NH_3 synthesis was investigated. Sivan *et al.* synthesized a series of Ru single atoms, clusters, and nanoparticles using a one-pot method to study the effect of Ru size on NH_3 synthesis.[86] The order of TOF was as follows: 2.8Ru–CeO_2 (Ru single atom and cluster) > 1.4Ru–CeO_2 (Ru single atom) > 4.0Ru–CeO_2 (Ru nanoparticle) > 5.3RuCeO_2 (Ru nanoparticle). It was suggested that the 2.8Ru–CeO_2 catalyst, which contained both Ru single atoms and clusters, can trigger NH_3 synthesis through the integration of dissociative and associative routes, resulting in excellent catalytic activity and stability. This work indicates that the combination of Ru single atom and cluster is a promising strategy to improve NH_3 synthesis performance.

In summary, recent researches have shown that the Ru cluster catalysts usually exhibit higher NH_3 synthesis rates than Ru nanoparticle catalysts. The potential reasons are summarized as follow: (1) the Ru cluster catalysts possess a higher metal dispersion and utilization than Ru nanoparticle catalysts; (2) the strong intra-cluster interaction of the Ru cluster can enhance the adsorption and activation of N_2 molecules; (3) the distinct reaction mechanism over Ru cluster catalysts compared with Ru nanoparticle catalysts enables facile NH_3 synthesis

under mild conditions. Nevertheless, the associative mechanism over Ru cluster catalysts is still controversial, which still require solid evidence to support this opinion. Therefore, there is an urgent need to develop more advanced characterization techniques such as time-of-flight secondary ion mass spectrometry (TOF-SIMS) and neutron technology to detect intermediate species and elucidate the reaction mechanism.

3.2 Non-noble metal SCCs

Theoretical calculations indicate that an ideal metal catalyst for NH_3 synthesis should have moderate adsorption energy of N atoms and NH_x desorption energy, namely, near the top position of the volcano diagram, such as the Ru metal.[87,88] In consideration of the scarcity and high price of Ru metal, there is an urgent need to develop catalysts with excellent catalytic performance, cost-effective or rich in Earth for NH_3 synthesis at mild conditions.[89] Liu et al. proposed an active center of Fe_3 clusters anchored on the Al_2O_3 (010) surface through first-principles calculations and microkinetic analysis (Fig. 6a).[47] The study found that the first hydrogenation of N_2 to generate NNH on the Fe_3/θ-Al_2O_3 (010) surface was much faster than the dissociative mechanism. The subsequent NNH dissociation also had a low energy barrier of 0.45 eV, thus bypassing the BEP relationship and the limitation on one the side of the volcano curve (Fig. 6b). Correspondingly, the calculated TOF of NH_3 synthesis on Fe_3/θ-Al_2O_3 (010) was comparable to that of Ru B_5 sites and was two orders of magnitude faster than the C_7 sites of Fe. These results indicated that surface-anchored metal trimers and/or multinuclear clusters might serve as efficient catalysts for NH_3 synthesis at mild conditions. Meanwhile, Luo et al. conducted a systematic study of NH_3 synthesis on triatomic metal clusters (M_3) of 20 transition metals.[90] The three key processes including N_2 dissociation, hydrogenation, and NH_3 desorption were calculated to evaluate the catalytic roles of

these M_3 clusters. The results showed that the transition metals can be divided into three categories (Fig. 6c): (1) N_2 can spontaneously dissociate on TMI-M_3 metals (i.e., Sc_3, Ti_3, V_3, Y_3, Zr_3, and Nb_3); (2) obvious activation barriers needed to be overcome on TMII-M_3 metal clusters (i.e., Cr_3, Mn_3, Fe_3, Co_3, Mo_3, Tc_3, Ru_3, and Rh_3); (3) and the activation process on TMIII-M_3 clusters (i.e., Ni_3, Cu_3, Zn_3, Pd_3, Ag_3, and Cd_3) was not feasible. Considering the three key processes for N_2 reduction to NH_3, four M_3 clusters in the TMI group (Y_3, Sc_3, Zr_3, and Nb_3) were proposed as ideal candidate clusters catalyst for NH_3 synthesis.

Beyond theoretical calculations, Peng et al. conducted research on the synthesis of NH_3 using non-precious metal cluster catalysts.[20] The cobalt atomic dimers on a nitrogen–carbon support (Co_2 ACCs) were synthesized for NH_3 synthesis and using the Co SAC and Ru NPS as references. Under 400 °C and 1 MPa, Co_2 ACCs exhibited a very high NH_3 synthesis rate of 8.54 $mmol_{NH_3}$ g_{cat}^{-1} h^{-1}, which is ~1.8- and 3.3-fold that of the Co SAC (4.60 $mmol_{NH_3}$ g_{cat}^{-1} h^{-1}) and Co NPs (2.55 $mmol_{NH_3}$ g_{cat}^{-1} h^{-1}), respectively. The low N_2 reaction order and the bands associated with N_2H_x intermediates in the in situ diffuse reflectance infrared Fourier-transform spectroscopy (DRIFTS) suggested that N_2 was not directly dissociated while it underwent the associative route for NH_3 synthesis (Fig. 6d and e).

Although there is currently limited research on non-precious metal cluster catalysts in NH_3 synthesis, theoretical studies indicate that non-precious metal cluster catalysts exhibit significant potential in this regard. The key challenge is to prepare uniform non-precious metal cluster catalysts with a specific number of atoms. Current methods for preparing atomic clusters include (1) using precursors containing specific atomic clusters; (2) anchoring atomic clusters on carrier materials with defect sites, such as C_3N_4 carriers; and (3) the application of atomic layer deposition (ALD). Besides, developing more efficient methods for preparing atomic cluster catalysts is of great significance.
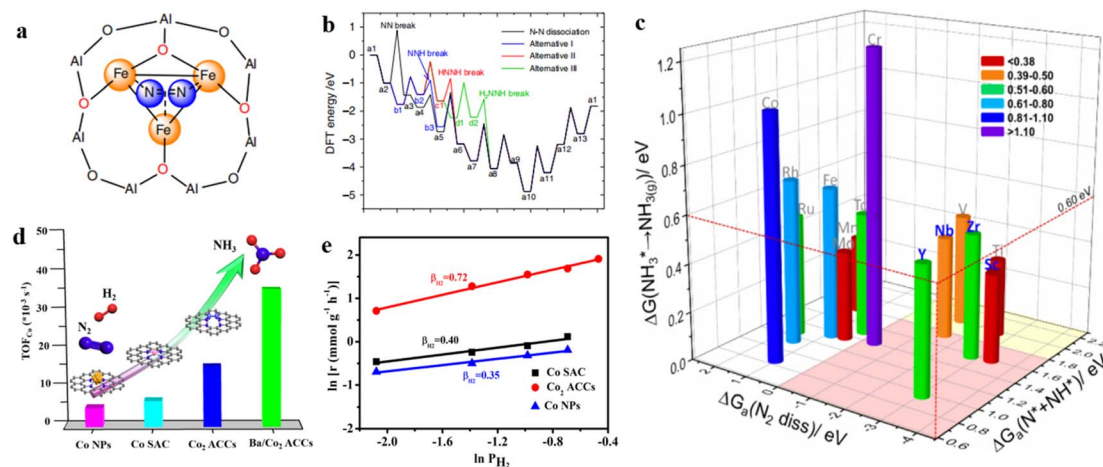
Fig. 6 (a) Schematic representation of N_2 coordinated with heterogeneous Fe_3/θ-Al_2O_3(010) in the same configuration; (b) the dissociative mechanism, and three pathways of associative mechanism with N−N bond dissociation at *NNH, *HNNH, and *HNNH$_2$ intermediates by the alternating hydrogenation route.[47] (c) Summary of the free energy of transition state for N_2 dissociation, hydrogenation barrier of *N + *NH formation, and desorption energy of NH_3 on 14 three-atom metal clusters.[90] (d) Turnover frequencies (TOF$_{Co\ total}$) at 400 °C and 1 MPa. (e) Reaction orders of H_2 over different catalysts at 400 °C and 1 MPa.[20]

4. BCCs for NH₃ synthesis

Apart from single-atom and single-cluster catalysts, bimetallic clusters have emerged as one of the important categories of heterogeneous catalyst. In many cases, bimetallic catalysts exhibit higher catalytic activity or selectivity than their mono-metallic counterpart due to the strong synergistic effect between different sites.[91,92] In NH₃ synthesis, it was reported that the dual-site strategy can effectively improve NH₃ synthesis performance owing to the separated sites for N₂ and H₂ activation, which can not only avoid the hydrogen poisonous over active sites caused by competition adsorption of N₂ and H₂, but also provide the possibility to circumvent the scale relations in NH₃ synthesis.[93,94] In addition, the bimetallic-cluster catalysts exhibit quite distinct properties in electronic and geometric structure compared with monometallic catalysts, which has a great impact on the reaction mechanism in NH₃ synthesis.[95] In general, according to the composition and structure of bimetallic catalysts, it can be classified into bimetallic-alloy catalysts, bimetallic single-cluster catalysts, and single-atom/dimer alloy catalysts.

4.1 Bimetallic-alloy catalysts

Because of high surface free energy, the Ru clusters are thermodynamically unstable and tend to sinter at high temperatures during NH₃ synthesis. In order to increase the stability of Ru clusters, Ni et al. reported a method to confine Co$_x$Ru$_y$ nanoparticles in the pores of N-doped carbon through the guiding of benzoic acid to restrict the deposition location of Ru and Co species.[96] The results of high-angle annular dark field scanning transmission electron microscopy (HAADF-STEM) showed that the Co$_x$Ru$_y$ alloy with an average size of 2.2–2.6 nm was confined inside the pores of N-doped carbon spheres. The catalytic activity test displayed that Co₁Ru₂/NC had a high NH₃ synthesis rate of 18.9 mmol$_{NH_3}$ g$_{cat}^{-1}$ h^{-1} at 400 °C and 3 MPa, which is 3.2-fold that of the Ru/NC catalyst (Fig. 7a). In addition, Co₁Ru₂/NC presented a relatively higher stability in NH₃ synthesis than Co₁Ru₂/NC-IWI prepared by traditional incipient wetness impregnation method (Fig. 7b), demonstrating that the confinement of Ru and Co NPs inside the hollow pores of N-doped carbon spheres can enhance the stability of RuCo alloy. In comparison with Ru–Co nanoparticles, Yang et al. developed a bimetallic Ru–Co clusters/N–C catalyst derived from a confined alloying process within zeolite–imidazolate frameworks (ZIF).[97] As shown in Fig. 7c, Ru₃(CO)₁₂ was introduced into the cavity of ZIFs that use the Co-bearing metal–organic frameworks as the host. After decomposition at 900 °C, the bimetallic Ru–Co clusters can be in situ formed. Fig. 7d showed that Ru–Co clusters@N–C possessed the highest NH₃ synthesis rate among Ru–Co NPs@N–C, Ru clusters@N–C, and Ru NPs@N–C catalysts. Compared with the Ru–Co NPs catalyst, the bimetallic Ru–Co clusters exhibited a higher density of low-coordination and unsaturated active sites, which may favor the adsorption and activation of N₂ molecules.
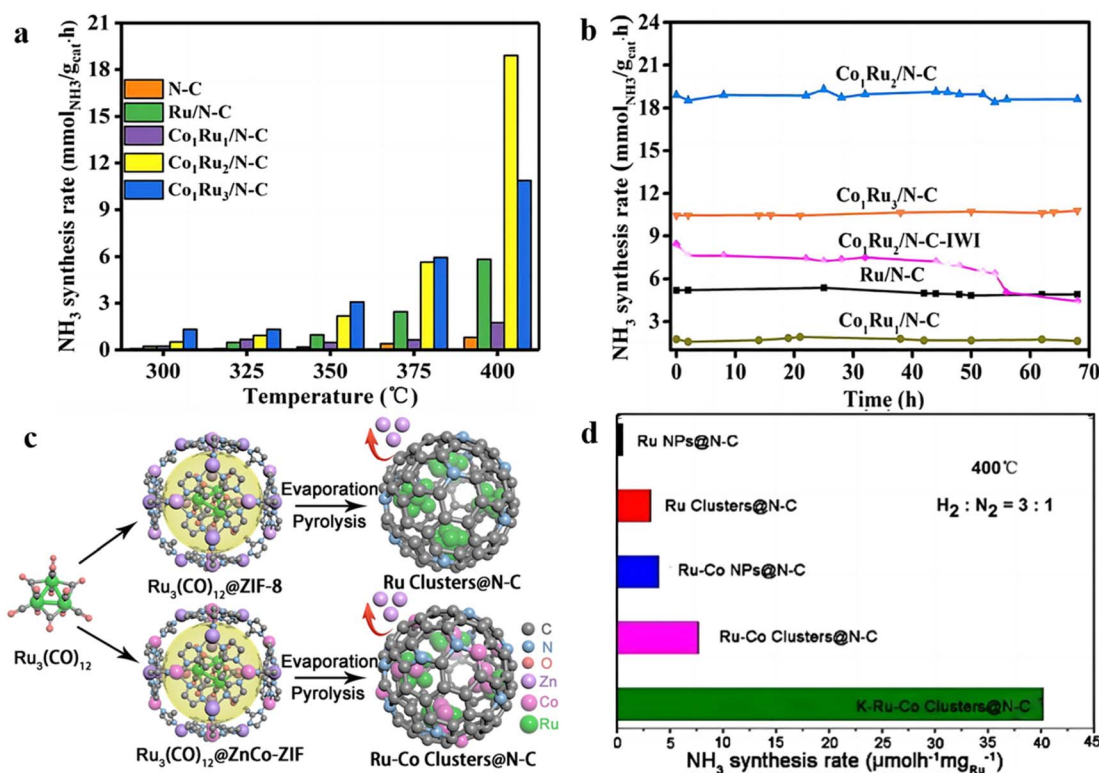

Fig. 7 (a) NH₃ synthesis rate over catalysts at 300–400 °C and 3 MPa. (b) Time dependence of NH₃ synthesis rate at 400 °C and 3 MPa.[96] (c) Schematic diagram of the preparation of Ru–Co clusters@N–C catalyst. (d) NH₃ synthesis rate over the as-prepared catalysts at 400 °C and 0.1 MPa.[97]

Besides, alloying with Co atoms would tailor the local structure of Ru clusters owing to the synergistic effect. As a result, the NH_3 synthesis rate over Ru–Co clusters@N–C is 2.4 times higher than that of Ru clusters@N–C. These results elucidate that bimetallic Ru–Co alloy can not only improve NH_3 synthesis rate but also increase the thermal stability compared with Ru nanoparticle catalysts.

4.2 Bimetallic single-cluster catalysts

Bimetallic single-cluster catalysts mean that one of the elements in bimetallic clusters is atomically dispersed.[98,99] The bimetallic single-cluster sites (M_1A_n) not merely possess the advantage of SACs with complete metal dispersion but also provide the possibility to overcome scaling relation through the cooperative effects of bimetallic sites that are responsible for different elementary steps. In NH_3 synthesis, Ma et al. explored the reaction mechanism of N_2-to-NH_3 thermal conversion on the bimetallic Rh_1Co_3 site using DFT calculation.[100] They found that the preferred reaction pathway over the Rh_1Co_3 site was the associative mechanism analogous to the biological process, which was driven by both the charge buffering ability of doped metal Rh in Rh_1Co_3 and the complementary role of Co in catalysis (Fig. 8a). Apart from the bimetallic single-cluster anchored on a metal oxide, the supported bimetallic single-cluster catalysts are also promising for NH_3 synthesis. Ru-loaded hydrides were reported to work as efficient catalysts

for NH_3 synthesis at low temperatures, where the formation of hydrogen vacancies (V_H) at the Ru/hydrides is a key factor for NH_3 synthesis. Nakao et al. investigated the V_H formation and H-migration behavior at the Ru-TM/Ca_2NH interface using the Ru_5TM/Ca_2NH model by DFT calculations (Fig. 8b).[101] It was revealed that the five late TMs (Fe, Co, Rh, Os, and Ir) and eight early TMs (Sc, Ti, Y, Zr, Nb, La, Hf, and Ta) were determined to promote V_H formation. In addition, Nb, Hf, Ta, Os, and Ir can also decrease the H-migration energy at the Ru_5TM/Ca_2NH interface when compared with that at the Ru_6/Ca_2NH interface. Therefore, the formation of bimetallic Ru_5TM clusters over hydrides via the addition of a proper TM atom can improve the NH_3 synthesis performance in terms of the V_H formation and H-migration energy. To unveil the synergy of bimetallic sites, Cheng et al. studied the Fe_{13} cluster and bimetallic $Fe_{12}X$ (X = V, Cr, Mn, Co, Ni, Cu, Zn, Nb, Mo, Ru, and Rh) clusters for NH_3 synthesis (Fig. 8c).[102] The energies analysis showed that center substitution ($X@Fe_{12}$) was favored while doping single V, Cr, Co, and Mo atoms, whereas Mn, Ni, Cu, Zn, Nb, Ru, and Rh tended to form shell-doped structures ($Fe_{12}X$). Among these bimetallic single clusters, $Fe_{12}Nb$ exhibited the lowest activation energy for N_2 dissociation and the dissociated *N species was converted into NH_3 efficiently via a hydrogenation process (Fig. 8d).

To be noted, although bimetallic single-cluster catalysts show great advantages for NH_3 synthesis on the basis of DFT calculations, the synthesis and application of bimetallic single-cluster catalysts in NH_3 synthesis have not been reported yet.
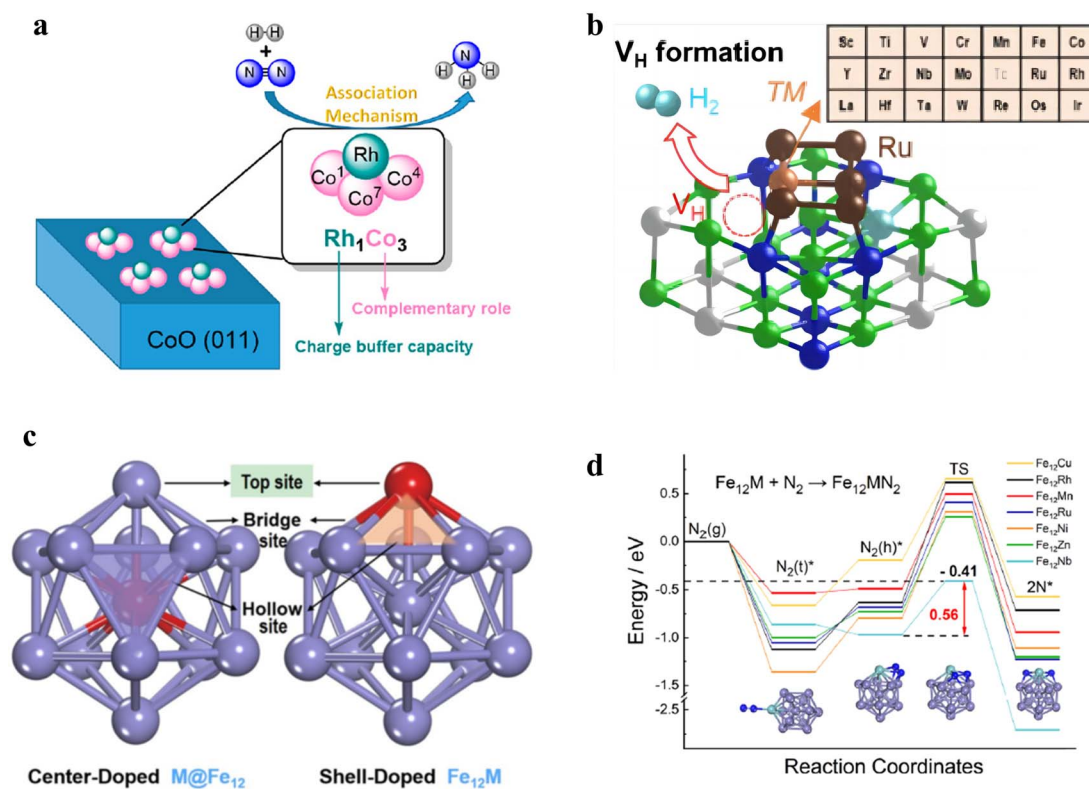

Fig. 8 (a) Schematic diagram of Rh_1Co_3 bimetallic sites for NH_3 synthesis.[100] (b) Schematic diagram of the Ru_5TM/Ca_2NH model.[101] (c) The chemical structure of heteroatom-doped Fe_{13} clusters. The red atoms represent the different doping positions.[102] (d) Pathways of N_2 adsorption and dissociation on the shell-doped $Fe_{12}TM$ clusters.

The main challenge lies in the preparation of uniform bimetallic clusters with specific structure, which requires the development of special preparation method and the application of advanced equipment. Besides, DFT calculations demonstrated that the reaction mechanism of NH_3 synthesis over bimetallic single-cluster catalysts is closely related to their composition and property. For instance, the preferred reaction pathway over the Rh_1Co_3 site is an associative mechanism, while that over the $Fe_{12}X$ (X = Mn, Ni, Cu, Zn, Nb, Ru, and Rh) site is dissociative mechanism. The real reaction mechanisms over different bimetallic single-cluster catalysts still need to be further confirmed by experimental research.

4.3 Single-atom/dimer alloy catalysts

Single-atom alloys (SAAs) are a class of bimetallic single-site heterogeneous catalyst in which small amounts of one metal are atomically dispersed in the surface of a different metal.[103,104] Distinguished from traditional metal alloy, the amount of guest metal atom in SAAs is small and the sites are isolated. Due to the unique geometry of SAAs, the location of the transition state and the binding site of reaction intermediates are often decoupled, which make it possible to enable both the facile dissociation of reactants and weak binding of the intermediates. For example, Zhang at el. reported a Co_1Ru SAA catalyst *via* the deposition of atomically dispersed Co onto the surface of Ru tiny subnanoclusters (TCs).[105] It was revealed that the special structure can generate a spatial effect and induce strong inter-electronic interactions between Ru and Co, which can lead to the simultaneous generation of the high-surface-unoccupied Co 3d charge and obvious upshifting of the Ru d-band center. Based on the special electronic and geometric structure, Co_1Ru TCs can promote N_2 activation with a low barrier energy and enable the repulsion to the adsorption of the N-containing intermediates on the catalyst surface, resulting in the weakening of the binding of $*NH_3$ and $*N_2H_4$ intermediates on the Co_1Ru TCs catalyst surface. In such a case, the scaling relation over Co_1Ru TCs in NH_3 synthesis was decoupled. As such, the developed Co_1Ru TCs presented a much higher NH_3 synthesis rate and lower reaction activation energy than those of Co_1Ru dual atoms (DAs) and Co_1Ru nanoparticles (NPs). Furthermore, Zhang *et al.* prepared a series of M_1Ru SAA catalysts by the anchoring of transition-metal single atom (Fe, Co, and Ni) onto Ru nanoclusters.[106] They found that Co_1Ru SAA has the highest NH_3 synthesis rate and the largest TOF_{Ru} value among various M_1Ru SAA (Fig. 9a). Compared with the CoRu nanoparticle alloy (NPA), various characterizations elucidated that Co_1Ru SAA possessed stronger electronic interaction between Co and Ru, which induced lower work function and up-shift d band center toward the Fermi level, thus accelerating the activation of N_2. Meanwhile, the unique SAA structure could effectively tune the N_2 activation pathway. DRIFTS technique showed that the $*N_2D_x$ intermediates can be observed over Co_1Ru SAA under the atmosphere of 25% N_2–75% D_2, demonstrating that N_2 molecules can be activated *via* an associative mechanism, accounting for efficient NH_3 synthesis at mild conditions (Fig. 9b).
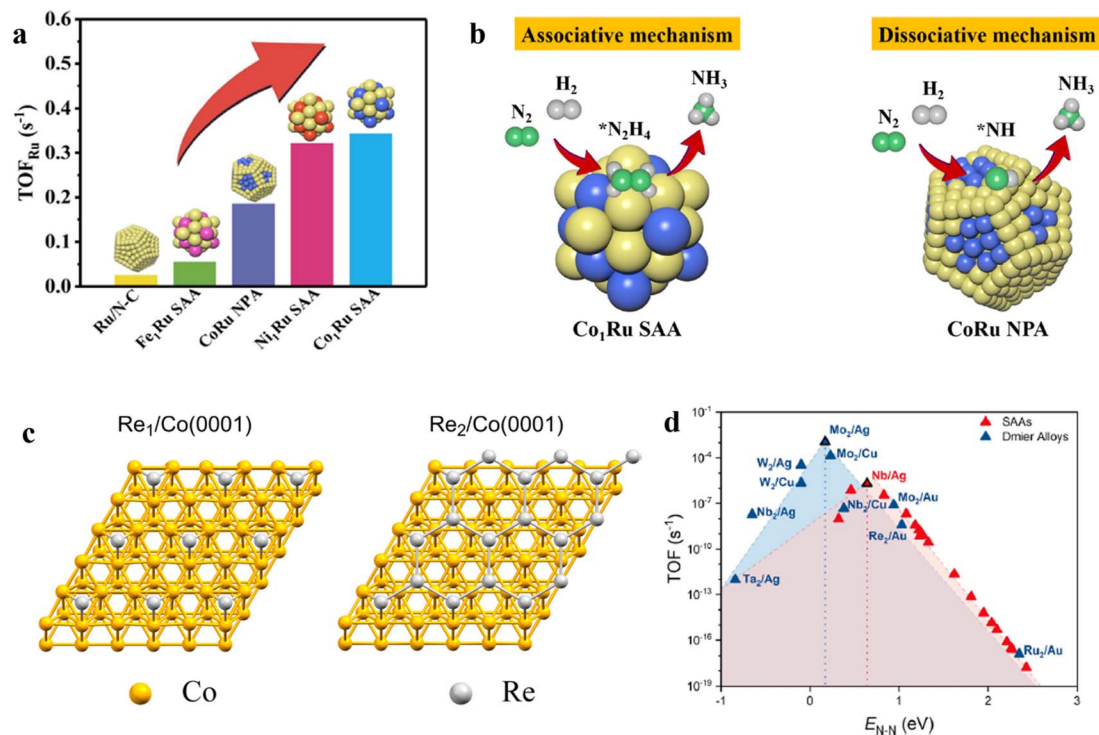
Fig. 9 (a) TOF_{Ru} values over the as-synthesized catalysts at 400 °C and 1 MPa. (b) The proposed N_2 activation pathway over Co_1Ru SAA and CoRu NPA.[106] (c) Top views of free Re_1 and Re_2 centers over Co(0001).[107] (d) Comparison of the volcano plot of TOF for dimer alloys and SAAs as a function of *N–N transition state energies.[107] The TOF is calculated at 673 K, P_{N_2} = 24.5 bar, P_{H_2} = 74.25 bar, P_{NH_3} = 1 bar, and 2% conversion to NH_3. TOFs of Mo_2/Au, Ru_2/Au, and Re_2/Au dimer alloys are calculated using the DFT results reported in ref. 109.

In addition, Cholach *et al.* investigated the active centers of one or a pair of Re atoms on the Co(0001) support for NH_3 synthesis using DFT calculation (Fig. 9c).[107] They found that the binding N to Re and Co can significantly reduce the heat of dissociative adsorption of N_2 in the cases of $Re_1/Co(0001)$, $Re_2/Co(0001)$, and Re(0001). As a result, the specific TOF on the basis of $Re_1/Co(0001)$, $Re_2/Co(0001)$, and the plane Re(0001) changed in the order of 8.0×10^3, 32.0, and 1.0, respectively. They also demonstrated that the Re single atom on the Co(0001) support exhibited a much higher NH_3 synthesis performance than that of Re dual atoms. Nevertheless, when the host metal was changed into either Cu(111) or Ag(111), the transition-metal single atom or dimer atoms supported on Ag(111) or Cu(111) catalysts presented different trends. Zhang *et al.* revealed that the Nb/Ag SAA was located at the volcano peak of NH_3 synthesis on the basis of the $TM_1/Ag(111)$ system, while the Mo_2/Ag dimer alloy exhibited a much higher TOF value compared with Nb/Ag SAA (Fig. 9d).[108] DFT calculations showed that the Mo_2/Ag dimer alloy has a lower N_2 activation energy and weaker N absorption than that of Nb/Ag SAA, *i.e.*, the BEP relationship for N_2 dissociation derived on dimer alloys is closer to the ideal limit in comparison to that obtained on SAAs, leading to the higher activities of dimer alloys for NH_3 synthesis.

Although M_1Ru SAAs have been reported to exhibit considerable NH_3 synthesis performance experimentally, while this kind of SAAs are based on the Ru as the host metal atoms in SAAs. The development of SAAs with single-atom Ru as the guest metal atom in SAAs for NH_3 synthesis is more appealing, especially for reducing the content of noble Ru metal. In addition, the predicted higher NH_3 synthesis performance of dimer alloys than SAAs provides a wide platform to exploit more efficient catalysts for NH_3 synthesis. Developing advanced methods for the preparation of dimer alloys is really worth exploring.

5. Conclusions and prospects

The development of efficient catalysts for NH_3 synthesis under mild conditions has been a long-term endeavor in this field. The remarkable differences in the geometric and electronic structure of active sites at different scales stimulate that the single-atom and cluster catalysts exhibit significantly distinct catalytic performance and reaction mechanism compared with nanoparticle catalysts. Based on the analysis in this review, the main differences between nanoparticle catalysts, single-atom and cluster catalysts are summarized by the following three aspects:

5.1 Hydrogen poisonous

Nanoparticle catalysts usually suffer from unavoidable hydrogen poisoning due to the strong adsorption of H species on the nanoparticle surface, while the hydrogen poisonous was

Table 1 Catalytic properties for NH_3 synthesis over various SACs, SCCs, and BCCs catalysts

Catalyst		Metal content (wt%)	Temperature (°C)	Pressure (MPa)	WHSV (mL g^{-1} h^{-1})	NH_3 synthesis rate (mmol$_{NH_3}$ g$_{cat}$$^{-1}$ h^{-1})	Ref.
			Reaction conditions				
SACs	Co–N–C	3.8	350	1.0	60 000	4.34	48
	Ba–Ru SAs/S-1	0.27	400	0.1	18 000	1.39	63
	Ru/HZ SAC	0.2	300	1.0	60 000	2.52	65
	MoH_x	2.0	400	0.1	12 000	0.026	72
	$Co–N_2$	3.2	300	1.0	60 000	2.7	69
	FeN4©G-K	2.1	190	0.1	30 000	10.3×10^{-3}	71
	$Ru/CeO_2(SAC)$	1.00	450	1.0	72 000	9.9	119
	Ru SAC	0.39	400	1.0	60 000	4.7	49
SCCs	1.4 nm Ru NCs	1.18	400	1.0	60 000	17.1	19
	2.0 nm Ru NCs	1.06	400	1.0	60 000	8.8	19
	$Ru_{3.0}/BaCeO_3$	0.44	400	1.0	60 000	3.4	75
	$Ru_{1.1}/BaCeO_3$	0.46	400	1.0	60 000	19.4	75
	Ru/MgO-MIL	3.00	400	1.0	15 000	4.5	76
	Ru clusters/CeO_2	5.00	400	1.0	—	28.0	79
	0.5Ru-SNCs	0.49	400	3.0	60 000	11.7	85
	Ru ACCs	0.40	400	1.0	60 000	7.4	49
	Ru-2.8 nm	0.44	400	1.0	60 000	2.9	49
	5% Ru/Sm_2O_3 (activated)	5.00	400	1.0	24 000	32.2	82
	Ru/Sm_2O_3	5.00	400	1.0	24 000	23.0	81
	Co_2 ACCs	0.90	400	1.0	60 000	8.5	20
	Ba/Co_2 ACCs	0.90	400	1.0	60 000	19.4	20
BCCs	Co_1Ru_2/NC	1.17Ru + 0.41Co	400	3.0	60 000	18.9	95
	Ru–Co clusters@N–C	—	400	1.0	12 000	0.78	96
	Ru clusters@N–C	—	400	1.0	12 000	0.32	96
	Co_1Ru SAA	1.05Ru + 0.30Co	400	1.0	60 000	4.38	105
	Fe_1Ru SAA	1.36Ru + 0.47Fe	400	1.0	60 000	0.70	105
	Ni_1Ru SAA	1.07Ru + 0.51Ni	400	1.0	60 000	2.90	105
	CoRu NPA	0.95Ru + 0.29Co	400	1.0	60 000	2.09	105

largely alleviated or eliminated on cluster catalysts.[110–112] The probable reasons may be attributed to that the emergence of discrete d and sp bands of cluster atoms can alter the adsorption strength of N_2 and H_2 molecules, avoiding hydrogen poisonous or the increased interface of the metal–support can promote the hydrogen spillover to support and thus eliminate hydrogen poisonous.[49,75]

5.2 Reaction mechanism

The dissociative mechanism is preferred to occur on nanoparticle catalysts because of the presence of multiple atomic sites, such as Ru B_5 sites or Fe C_7 sites, which are highly active for the dissociation of N_2 molecules.[31,33] In terms of single-atom and cluster catalysts, the associative mechanism is suggested to be dominant even though satisfactory evidence is still needed to support this opinion.

5.3 Catalytic performance

By comparing the performance of different-size catalysts (Table 1), the cluster catalysts exhibit higher NH_3 synthesis rates than nanoparticle catalysts and single-atom catalysts thanks to the exposure of more active sites and/or different reaction mechanisms.[49,113] Concerning single-atom catalysts, the NH_3 synthesis rates are generally low in spite of their high dispersion.[113,114] The underlying reason could be the difficulty of simultaneous activation of N_2 and H_2 reactants on a single-atom site. To be noted, Ru species exist as large nanoparticles ($\geq$2 nm) in industrial Ru-based catalysts. The higher catalytic performance of Ru clusters than Ru particles makes it possible to reduce the Ru content of commercial catalysts in the form of stable Ru clusters.

It is worth noting that the exploitation of single-atom and cluster catalysts for NH_3 synthesis with high-efficiency has gained more and more attention. With the advancement of preparation method and characterization techniques, an increasing number of single-atom and cluster catalysts would be developed for NH_3 synthesis. In the future, some research fields in terms of single-atom and cluster catalysts are promising to further improve the catalyst performance and deepen the fundamental understanding of structure–activity relationship as well as the reaction mechanism for NH_3 synthesis.

Fabricating the uniform active sites in SCCs or BCCs is still a great challenge. In terms of performance for NH_3 synthesis, SCCs or BCCs are superior to SACs and nanoparticle catalysts. Nevertheless, the preparation of uniform and exclusive structural SCCs or BCCs is much more difficult than SACs and nanoparticle catalysts, and most researches on SCCs or BCCs were based on DFT calculations. Currently, the widely used synthesis methods for SCCs or BCCs are the control of low metal loading or high-temperature pyrolysis, which are the lack of the precise manipulation of the location of metal species. With the usage of organometallic complex precursors containing atomic clusters and the application of advanced methods and instruments, it provides the possibility to precisely control the configuration and location of atomic clusters. Meanwhile, the precise construction of cluster sites can not only maximize

metal utilization but also provide platforms to investigate the reaction mechanism.

To better characterize the structure of single-atom and cluster catalysts as well as to detect the reaction intermediate species, it is necessary to develop advanced characterization techniques. Nowadays, the reaction mechanisms via the associative or dissociative pathway of single-atom and cluster catalysts are still under debate. The intermediates for NH_3 synthesis, such as NH_x and N_2H_x species, are mainly detected by the UV-vis spectrum, in situ DRIFTS, and NEXAFS spectra.[85,115,116] The main reason is due to that these techniques would be possible to detect only those long-lived intermediates, which can give rise to a detectable population under steady-state conditions. Meanwhile, it is also difficult to accurately distinguish the spatial distribution of intermediates over different active sites based on in situ DRIFTS and NEXAFS spectra. The development of advanced characterization techniques, such as near ambient pressure X-ray photoelectron spectroscopy (NAP-XPS), TOF-SIMS, and neutron scattering techniques, would shed light on the analysis of catalyst structure and reaction mechanism in NH_3 synthesis.

The industrial application of NH_3 synthesis via an associative mechanism still faces long-term challenges, mainly focusing on the accessibility and durability of catalysts. Specifically, the application of catalysts with highly dispersed active sites is trapped in the metal agglomeration, i.e., the growth of metal size from subnanometer to nanometer in the long-period operation. As a result, the NH_3 synthesis mechanism is changed from associative route to dissociative route during the reaction process, possibly accompanied by the decrease in the NH_3 synthesis rate. Moreover, the large-scale preparation of single-atom and cluster catalysts in the industry is still tough because of the complicated synthetic method and the difficulty of controlling the homogeneous dispersion of low-loading metal. Therefore, more efforts are needed to solve the stability and large-scale preparation of advanced single-atom and cluster catalysts before industrial application.

Artificial intelligence (Ai)-assisted catalyst design will accelerate the development of efficient single-atom and cluster catalysts for NH_3 synthesis.[117,118] Traditional catalysts were discovered through trial-and-error method coupled with chemical intuition. In the early days of NH_3 synthesis research, thousands of catalysts were prepared and tested to find a catalyst suitable for industrialization. Nowadays, we are still trying new types of catalysts in order to improve the NH_3 synthesis activity at lower temperatures and pressure conditions. With the assistance of artificial intelligence, especially for automatic machine-learning, it shows enormous potential to accelerate the predictive discovery of novel catalyst formulations. Meanwhile, the combination of machine-learning methodology and high-throughput experimentation can greatly shorten the period of discovery of efficient catalysts for NH_3 synthesis.

Author contributions

Conceptualization, investigation and writing – original draft: X. Peng, M. Zhang and T. Zhang. Conceptualization and writing –

Conflicts of interest

The authors declare no conflict of interest.

Acknowledgements

References

1 Z. W. Seh, J. Kibsgaard, C. F. Dickens, I. Chorkendorff, J. K. Nørskov and T. F. Jaramillo, Combining theory and experiment in electrocatalysis: insights into materials design, *Science*, 2017, **355**, eaad4998.

2 K. Mazloomi and C. Gomes, Hydrogen as an energy carrier: prospects and challenges, *Renewable Sustainable Energy Rev.*, 2012, **16**, 3024–3033.

3 Y. Kojima and M. Yamaguchi, Ammonia as a hydrogen energy carrier, *Int. J. Hydrogen Energy*, 2022, **47**, 22832–22839.

4 P. Wang, H. Xie, J. Guo, Z. Zhao, X. Kong, W. Gao, F. Chang, T. He, G. Wu and M. Chen, The formation of surface lithium–iron ternary hydride and its function on catalytic ammonia synthesis at low temperatures, *Angew. Chem., Int. Ed.*, 2017, **129**, 8842–8846.

5 T.-N. Ye, S.-W. Park, Y. Lu, J. Li, J. Wu, M. Sasase, M. Kitano and H. Hosono, Dissociative and associative concerted mechanism for ammonia synthesis over Co-based catalyst, *J. Am. Chem. Soc.*, 2021, **143**, 12857–12866.

6 C. Zamfirescu and I. Dincer, Using ammonia as a sustainable fuel, *J. Power Sources*, 2008, **185**, 459–465.

7 C. H. Christensen, T. Johannessen, R. Z. Sørensen and J. K. Nørskov, Towards an ammonia-mediated hydrogen economy, *Catal. Today*, 2006, **111**, 140–144.

8 N. Kuganathan, H. Hosono, A. L. Shluger and P. V. Sushko, Enhanced N_2 dissociation on Ru-loaded inorganic electride, *J. Am. Chem. Soc.*, 2014, **136**, 2216–2219.

9 H. Liu, Ammonia synthesis catalyst 100 years: practice, enlightenment and challenge, *Chin. J. Catal.*, 2014, **35**, 1619–1640.

10 K. Sato and K. Nagaoka, Boosting ammonia synthesis under mild reaction conditions by precise control of the basic oxide–Ru interface, *Chem. Lett.*, 2021, **50**, 687–696.

11 J. Wang, L. Yu, L. Hu, G. Chen, H. Xin and X. Feng, Ambient ammonia synthesis *via* palladium-catalyzed electrohydrogenation of dinitrogen at low overpotential, *Nat. Commun.*, 2018, **9**, 1795–1802.

12 T. Ogawa, Y. Kobayashi, H. Mizoguchi, M. Kitano, H. Abe, T. Tada, Y. Toda, Y. Niwa and H. Hosono, High electron density on Ru in intermetallic YRu$_2$: the application to catalyst for ammonia synthesis, *J. Phys. Chem. C*, 2018, **122**, 10468–10475.

13 A. Vojvodic, A. J. Medford, F. Studt, F. Abild-Pedersen, T. S. Khan, T. Bligaard and J. Nørskov, Exploring the limits: a low-pressure, low-temperature Haber–Bosch process, *Chem. Phys. Lett.*, 2014, **598**, 108–112.

14 M. Kitano, Y. Inoue, Y. Yamazaki, F. Hayashi, S. Kanbara, S. Matsuishi, T. Yokoyama, S.-W. Kim, M. Hara and H. Hosono, Ammonia synthesis using a stable electride as an electron donor and reversible hydrogen store, *Nat. Chem.*, 2012, **4**, 934–940.

15 J. Qian, Q. An, A. Fortunelli, R. J. Nielsen and W. A. Goddard III, Reaction mechanism and kinetics for ammonia synthesis on the Fe (111) surface, *J. Am. Chem. Soc.*, 2018, **140**, 6288–6297.

16 J. W. Erisman, M. A. Sutton, J. Galloway, Z. Klimont and W. Winiwarter, How a century of ammonia synthesis changed the world, *Nat. Geosci.*, 2008, **1**, 636–639.

17 G. Xu, C. Cai and T. Wang, Toward Sabatier optimal for ammonia synthesis with paramagnetic phase of ferromagnetic transition metal catalysts, *J. Am. Chem. Soc.*, 2022, **144**, 23089–23095.

18 J. Wang, W. Cui, Q. Liu, Z. Xing, A. M. Asiri and X. Sun, Recent progress in cobalt-based heterogeneous catalysts for electrochemical water splitting, *Adv. Mater.*, 2016, **28**, 215–230.

19 X. Peng, X. Chen, Y. Zhou, F. Sun, T. Zhang, L. Zheng, L. Jiang and X. Wang, Size-dependent activity of supported Ru catalysts for ammonia synthesis at mild conditions, *J. Catal.*, 2022, **408**, 98–108.

20 X. Peng, H. Cai, Y. Zhou, J. Ni, X. Wang, B. Lin, J. Lin, L. Zheng, C.-t. Au and L. Jiang, Studies of a highly active cobalt atomic cluster catalyst for ammonia synthesis, *ACS Sustain. Chem. Eng.*, 2022, **10**, 1951–1960.

21 M. A. Shipman and M. D. Symes, Recent progress towards the electrosynthesis of ammonia from sustainable resources, *Catal. Today*, 2017, **286**, 57–68.

22 G. Ertl, Reactions at surfaces: from atoms to complexity (Nobel lecture), *Angew. Chem., Int. Ed.*, 2008, **47**, 3524–3535.

23 M. J. Bezdek and P. J. Chirik, Expanding boundaries: N_2 cleavage and functionalization beyond early transition metals, *Angew. Chem., Int. Ed.*, 2016, **55**, 7892–7896.

24 H.-P. Jia and E. A. Quadrelli, Mechanistic aspects of dinitrogen cleavage and hydrogenation to produce ammonia in catalysis and organometallic chemistry: relevance of metal hydride bonds and dihydrogen, *Chem. Soc. Rev.*, 2014, **43**, 547–564.

25 S. Zhang, Y. Zhao, R. Shi, G. I. Waterhouse and T. Zhang, Photocatalytic ammonia synthesis: recent progress and future, *EnergyChem*, 2019, **1**, 100013.

26 L. Ouyang, J. Liang, Y. Luo, D. Zheng, S. Sun, Q. Liu, M. S. Hamdy, X. Sun and B. Ying, Recent advances in electrocatalytic ammonia synthesis, *Chin. J. Catal.*, 2023, **50**, 6–44.

27 J. Zhao and Z. Chen, Single Mo atom supported on defective boron nitride monolayer as an efficient electrocatalyst for

nitrogen fixation: a computational study, *J. Am. Chem. Soc.*, 2017, **139**, 12480–12487.

28 P. Emmett and S. Brunauer, The adsorption of nitrogen by iron synthetic ammonia catalysts, *J. Am. Chem. Soc.*, 1934, **56**, 35–41.

29 G. Ertl, Surface science and catalysis-studies on the mechanism of ammonia synthesis: the PH Emmett award address, *Catal. Rev.: Sci. Eng.*, 1980, **21**, 201–223.

30 G. Ertl, Elementary steps in heterogeneous catalysis, *Angew. Chem., Int. Ed.*, 1990, **29**, 1219–1227.

31 D. R. Strongin, J. Carrazza, S. R. Bare and G. A. Somorjai, The importance of C_7 sites and surface roughness in the ammonia synthesis reaction over iron, *J. Catal.*, 1987, **103**, 213–215.

32 K. Reuter, C. P. Plaisance, H. Oberhofer and M. Andersen, Perspective: on the active site model in computational catalyst screening, *J. Chem. Phys.*, 2017, **146**, 040901.

33 K. Honkala, A. Hellman, I. Remediakis, A. Logadottir, A. Carlsson, S. Dahl, C. H. Christensen and J. K. Nørskov, Ammonia synthesis from first-principles calculations, *Science*, 2005, **307**, 555–558.

34 N. Spencer, R. Schoonmaker and G. A. Somorjai, Iron single crystals as ammonia synthesis catalysts: effect of surface structure on catalyst activity, *J. Catal.*, 1982, **74**, 129–135.

35 D. Strongin, S. Bare and G. A. Somorjai, The effects of aluminum oxide in restructuring iron single crystal surfaces for ammonia synthesis, *J. Catal.*, 1987, **103**, 289–301.

36 D. Strongin and G. A. Somorjai, The effects of potassium on ammonia synthesis over iron single-crystal surfaces, *J. Catal.*, 1988, **109**, 51–60.

37 G. A. Somorjai and N. Materer, Surface structures in ammonia synthesis, *Top. Catal.*, 1994, **1**, 215–231.

38 J. J. Mortensen, L. B. Hansen, B. Hammer and J. K. Nørskov, Nitrogen adsorption and dissociation on Fe (111), *J. Catal.*, 1999, **182**, 479–488.

39 S. Dahl, A. Logadottir, R. Egeberg, J. Larsen, I. Chorkendorff, E. Törnqvist and J. K. Nørskov, Role of steps in N_2 activation on Ru (0001), *Phys. Rev. Lett.*, 1999, **83**, 1814–1819.

40 S. Dahl, E. Törnqvist and I. Chorkendorff, Dissociative adsorption of N_2 on Ru (0001): a surface reaction totally dominated by steps, *J. Catal.*, 2000, **192**, 381–390.

41 S. Dahl, J. Sehested, C. Jacobsen, E. Törnqvist and I. Chorkendorff, Surface science based microkinetic analysis of ammonia synthesis over ruthenium catalysts, *J. Catal.*, 2000, **192**, 391–399.

42 J. M. G. Carballo, J. Yang, A. Holmen, S. García-Rodríguez, S. Rojas, M. Ojeda and J. L. G. Fierro, Catalytic effects of ruthenium particle size on the Fischer–Tropsch synthesis, *J. Catal.*, 2011, **284**, 102–108.

43 H. Fang, D. Liu, Y. Luo, Y. Zhou, S. Liang, X. Wang, B. Lin and L. Jiang, Challenges and opportunities of Ru-based catalysts toward the synthesis and utilization of ammonia, *ACS Catal.*, 2022, **12**, 3938–3954.

44 P. Wang, F. Chang, W. Gao, J. Guo, G. Wu, T. He and P. Chen, Breaking scaling relations to achieve low-temperature ammonia synthesis through LiH-mediated nitrogen transfer and hydrogenation, *Nat. Chem.*, 2017, **9**, 64–70.

45 Y. Gong, J. Wu, M. Kitano, J. Wang, T.-N. Ye, J. Li, Y. Kobayashi, K. Kishida, H. Abe, Y. Niwa, H. Yang, T. Tada and H. Hosono, Ternary intermetallic LaCoSi as a catalyst for N_2 activation, *Nat. Catal.*, 2018, **1**, 178–185.

46 Y. Kobayashi, Y. Tang, T. Kageyama, H. Yamashita, N. Masuda, S. Hosokawa and H. Kageyama, Titanium-based hydrides as heterogeneous catalysts for ammonia synthesis, *J. Am. Chem. Soc.*, 2017, **139**, 18240–18246.

47 J.-C. Liu, X.-L. Ma, Y. Li, Y.-G. Wang, H. Xiao and J. Li, Heterogeneous Fe_3 single-cluster catalyst for ammonia synthesis *via* an associative mechanism, *Nat. Commun.*, 2018, **9**, 1610–1619.

48 X. Wang, X. Peng, W. Chen, G. Liu, A. Zheng, L. Zheng, J. Ni, C.-t. Au and L. Jiang, Insight into dynamic and steady-state active sites for nitrogen activation to ammonia by cobalt-based catalyst, *Nat. Commun.*, 2020, **11**, 653–663.

49 L. Li, Y.-F. Jiang, T. Zhang, H. Cai, Y. Zhou, B. Lin, X. Lin, Y. Zheng, L. Zheng and X. Wang, Size sensitivity of supported Ru catalysts for ammonia synthesis: from nanoparticles to subnanometric clusters and atomic clusters, *Chem*, 2022, **8**, 749–768.

50 J. Li, Y. Li and T. Zhang, Recent progresses in the research of single-atom catalysts, *Sci. China Mater.*, 2020, **63**, 889–891.

51 E. C. Tyo and S. Vajda, Catalysis by clusters with precise numbers of atoms, *Nat. Nanotechnol.*, 2015, **10**, 577–588.

52 Q. Yang, Y. Jiang, H. Zhuo, E. M. Mitchell and Q. Yu, Recent progress of metal single-atom catalysts for energy applications, *Nano Energy*, 2023, 108404.

53 B. Qiao, A. Wang, X. Yang, L. F. Allard, Z. Jiang, Y. Cui, J. Liu, J. Li and T. Zhang, Single-atom catalysis of CO oxidation using Pt_1/FeO_x, *Nat. Chem.*, 2011, **3**, 634–641.

54 Y. Zhou, F. Wei, H. Qi, Y. Chai, L. Cao, J. Lin, Q. Wan, X. Liu, Y. Xing and S. Lin, Peripheral-nitrogen effects on the Ru_1 centre for highly efficient propane dehydrogenation, *Nat. Catal.*, 2022, **5**, 1145–1156.

55 Q. He, Y. Meng, H. Zhang, Y. Zhang, Q. Sun, T. Gan, H. Xiao, X. He and H. Ji, Amino-metalloporphyrin polymers derived Fe single atom catalysts for highly efficient oxygen reduction reaction, *Sci. China: Chem.*, 2020, **63**, 810–817.

56 F. Chen, X. Jiang, L. Zhang, R. Lang and B. Qiao, Single-atom catalysis: bridging the homo-and heterogeneous catalysis, *Chin. J. Catal.*, 2018, **39**, 893–898.

57 Y. Wang, L. Chen, Z. Mao, L. Peng, R. Xiang, X. Tang, J. Deng, Z. Wei and Q. Liao, Controlled synthesis of single cobalt atom catalysts *via* a facile one-pot pyrolysis for efficient oxygen reduction and hydrogen evolution reactions, *Sci. Bull.*, 2019, **64**, 1095–1102.

58 J. Liu, H. Lu, D. W. Zhang and M. Nolan, Reactions of ruthenium cyclopentadienyl precursor in the metal precursor pulse of Ru atomic layer deposition, *J. Mater. Chem. C*, 2021, **9**, 2919–2932.

59 A. Wang, J. Li and T. Zhang, Heterogeneous single-atom catalysis, *Nat. Rev. Chem*, 2018, **2**, 65–81.

60 F. Huang, Y. Deng, Y. Chen, X. Cai, M. Peng, Z. Jia, P. Ren, D. Xiao, X. Wen and N. Wang, Atomically dispersed Pd on nanodiamond/graphene hybrid for selective hydrogenation of acetylene, *J. Am. Chem. Soc.*, 2018, **140**, 13142–13146.

61 X. Cui, X. Dai, A.-E. Surkus, K. Junge, C. Kreyenschulte, G. Agostini, N. Rockstroh and M. Beller, Zinc single atoms on N-doped carbon: an efficient and stable catalyst for CO_2 fixation and conversion, *Chin. J. Catal.*, 2019, **40**, 1679–1685.

62 J. M. Thomas, Tens of thousands of atoms replaced by one, *Nature*, 2015, **525**, 325–326.

63 J.-Z. Qiu, J. Hu, J. Lan, L.-F. Wang, G. Fu, R. Xiao, B. Ge and J. Jiang, Pure siliceous zeolite-supported Ru single-atom active sites for ammonia synthesis, *Chem. Mater.*, 2019, **31**, 9413–9421.

64 Á. Logadóttir and J. K. Nørskov, Ammonia synthesis over a Ru (0001) surface studied by density functional calculations, *J. Catal.*, 2003, **220**, 273–279.

65 X. Wang, L. Li, Z. Fang, Y. Zhang, J. Ni, B. Lin, L. Zheng, C.-t. Au and L. Jiang, Atomically dispersed Ru catalyst for low-temperature nitrogen activation to ammonia via an associative mechanism, *ACS Catal.*, 2020, **10**, 9504–9514.

66 F. Rosowski, A. Hornung, O. Hinrichsen, D. Herein, M. Muhler and G. Ertl, Ruthenium catalysts for ammonia synthesis at high pressures: preparation, characterization, and power-law kinetics, *Appl. Catal., A*, 1997, **151**, 443–460.

67 X. Wang, X. Peng, H. Ran, B. Lin, J. Ni, J. Lin and L. Jiang, Influence of Ru substitution on the properties of $LaCoO_3$ catalysts for ammonia synthesis: XAFS and XPS studies, *Ind. Eng. Chem. Res.*, 2018, **57**, 17375–17383.

68 A. Han, B. Wang, A. Kumar, Y. Qin, J. Jin, X. Wang, C. Yang, B. Dong, Y. Jia and J. Liu, Recent advances for MOF-derived carbon-supported single-atom catalysts, *Small Methods*, 2019, **3**, 1800471–1800492.

69 Y. Zhou, C. Wang, X. Peng, T. Zhang, X. Wang, Y. Jiang, H. Qi, L. Zheng, J. Lin and L. Jiang, Boosting efficient ammonia synthesis over atomically dispersed Co-based catalyst via the modulation of geometric and electronic structures, *CCS Chem.*, 2022, **4**, 1758–1769.

70 X. Li, Y. Jiao, Y. Cui, C. Dai, P. Ren, C. Song and X. Ma, Synergistic catalysis of the synthesis of ammonia with Co-based catalysts and plasma: from nanoparticles to a single atom, *ACS Appl. Mater. Interfaces*, 2021, **13**, 52498–52507.

71 Z. Chen, Y. Ye, T. Peng, C. Wu, H. Li, X. Pan and X. Bao, Iron-single sites confined by graphene lattice for ammonia synthesis under mild conditions, *ACS Catal.*, 2023, **13**, 14385–14394.

72 L. M. Azofra, N. Morlanés, A. Poater, M. K. Samantaray, B. Vidjayacoumar, K. Albahily, L. Cavallo and J. M. Basset, Single-site molybdenum on solid support materials for catalytic hydrogenation of N_2-into-NH_3, *Angew. Chem., Int. Ed.*, 2018, **57**, 15812–15816.

73 B. Lin, Y. Wu, B. Fang, C. Li, J. Ni, X. Wang, J. Lin and L. Jiang, Ru surface density effect on ammonia synthesis activity and hydrogen poisoning of ceria-supported Ru catalysts, *Chin. J. Catal.*, 2021, **42**, 1712–1723.

74 C. J. H. Jacobsen, S. Dahl, P. L. Hansen, E. Törnqvist, L. Jensen, H. Topsøe, D. V. Prip, P. B. Møenshaug and I. Chorkendorff, Structure sensitivity of supported ruthenium catalysts for ammonia synthesis, *J. Mol. Catal. A: Chem.*, 2000, **163**, 19–26.

75 Y. Zhou, J. Wang, L. Liang, Q. Sai, J. Ni, C.-t. Au, X. Lin, X. Wang, Y. Zheng, L. Zheng and L. Jiang, Unraveling the size-dependent effect of Ru-based catalysts on ammonia synthesis at mild conditions, *J. Catal.*, 2021, **404**, 501–511.

76 J. Li, W. Wang, W. Chen, Q. Gong, J. Luo, R. Lin, H. Xin, H. Zhang, D. Wang, Q. Peng, W. Zhu, C. Chen and Y. Li, Sub-nm ruthenium cluster as an efficient and robust catalyst for decomposition and synthesis of ammonia: break the "size shackles", *Nano Res.*, 2018, **11**, 4774–4785.

77 L. D. Marks, Experimental studies of small particle structures, *Rep. Prog. Phys.*, 1994, **57**, 603–649.

78 F. Tao, S. Dag, L.-W. Wang, Z. Liu, D. R. Butcher, H. Bluhm, M. Salmeron and G. A. Somorjai, Break-up of stepped platinum catalyst surfaces by high CO coverage, *Science*, 2010, **327**, 850–853.

79 J. Feng, L. Liu, X. Ju, M. Wang, X. Zhang, J. Wang and P. Chen, Sub-nanometer Ru clusters on ceria nanorods as efficient catalysts for ammonia synthesis under mild conditions, *ACS Sustain. Chem. Eng.*, 2022, **10**, 10181–10191.

80 S. Hirabayashi, M. Ichihashi and Y. Takeda, Optimization of ruthenium particle size and ceria support for enhanced activity of Ru/CeO_2 cluster catalysts in ammonia synthesis under mild conditions, *Catal. Lett.*, 2023, **154**, 487–493.

81 J. Wang, L. Liu, X. Zhang, J. Yu, X. Ju, J. Feng, J. Guo, T. He and P. Chen, Sub-nanometer Ru clusters on Sm_2O_3 obtained from a room temperature ion adsorption method for ammonia synthesis, *Catal. Sci. Technol.*, 2022, **12**, 7501–7509.

82 X. Zhang, L. Liu, A. Wu, J. Zhu, R. Si, J. Guo, R. Chen, Q. Jiang, X. Ju and J. Feng, Synergizing surface hydride species and Ru clusters on Sm_2O_3 for efficient ammonia synthesis, *ACS Catal.*, 2022, **12**, 2178–2190.

83 Y. Zhang, S. Li, C. Sun, X. Cao, X. Wang and J. Yao, Defective g-C_3N_4 supported Ru_3 single-cluster catalyst for ammonia synthesis through parallel reaction pathways, *Nano Res.*, 2023, **16**, 3580–3587.

84 Q.-Y. Fan, J.-L. Liu, F.-Q. Gong, Y. Wang and J. Cheng, Structural dynamics of Ru clusters during nitrogen dissociation in ammonia synthesis, *Phys. Chem. Chem. Phys.*, 2022, **24**, 10820–10825.

85 Y. Zhou, Q. Sai, Z. Tan, C. Wang, X. Wang, B. Lin, J. Ni, J. Lin and L. Jiang, Highly efficient subnanometer Ru-based catalyst for ammonia synthesis via an associative mechanism, *Chin. J. Chem. Eng.*, 2022, **43**, 177–184.

86 S. E. Sivan, K. H. Kang, S. J. Han, O. Francis Ngome Okello, S.-Y. Choi, V. Sudheeshkumar, R. W. J. Scott, H.-J. Chae, S. Park and U. H. Lee, Facile MOF-derived one-pot synthetic approach toward Ru single atoms, nanoclusters, and nanoparticles dispersed on CeO_2 supports for enhanced ammonia synthesis, *J. Catal.*, 2022, **408**, 316–328.

87 T. Bligaard, J. K. Nørskov, S. Dahl, J. Matthiesen, C. H. Christensen and J. Sehested, The Brønsted–Evans–Polanyi relation and the volcano curve in heterogeneous catalysis, *J. Catal.*, 2004, **224**, 206–217.

88 S. Dahl, A. Logadottir, C. J. H. Jacobsen and J. K. Nørskov, Electronic factors in catalysis: the volcano curve and the effect of promotion in catalytic ammonia synthesis, *Appl. Catal., A*, 2001, **222**, 19–29.

89 A. J. Medford, A. Vojvodic, J. S. Hummelshøj, J. Voss, F. Abild-Pedersen, F. Studt, T. Bligaard, A. Nilsson and J. K. Nørskov, From the Sabatier principle to a predictive theory of transition-metal heterogeneous catalysis, *J. Catal.*, 2015, **328**, 36–42.

90 C. Cui, H. Zhang, R. Cheng, B. Huang and Z. Luo, On the nature of three-atom metal cluster catalysis for N_2 reduction to ammonia, *ACS Catal.*, 2022, **12**, 14964–14975.

91 L. Liu, M. Lopez-Haro, C. W. Lopes, S. Rojas-Buzo, P. Concepcion, R. Manzorro, L. Simonelli, A. Sattler, P. Serna, J. J. Calvino and A. Corma, Structural modulation and direct measurement of subnanometric bimetallic PtSn clusters confined in zeolites, *Nat. Catal.*, 2020, **3**, 628–638.

92 X. Li, Y. Zhou, B. Qiao, X. Pan, C. Wang, L. Cao, L. Li, J. Lin and X. Wang, Enhanced stability of Pt/Al_2O_3 modified by Zn promoter for catalytic dehydrogenation of ethane, *J. Energy Chem.*, 2020, **51**, 14–20.

93 T. N. Ye, S. W. Park, Y. Lu, J. Li, M. Sasase, M. Kitano, T. Tada and H. Hosono, Vacancy-enabled N_2 activation for ammonia synthesis on an Ni-loaded catalyst, *Nature*, 2020, **583**, 391–395.

94 T. N. Ye, S. W. Park, Y. Lu, J. Li, J. Wu, M. Sasase, M. Kitano and H. Hosono, Dissociative and associative concerted mechanism for ammonia synthesis over Co-based catalyst, *J. Am. Chem. Soc.*, 2021, **143**, 12857–12866.

95 L. Nguyen, S. Zhang, L. Wang, Y. Li, H. Yoshida, A. Patlolla, S. Takeda, A. I. Frenkel and F. Tao, Reduction of nitric oxide with hydrogen on catalysts of singly dispersed bimetallic sites Pt_1Co_m and Pd_1Co_n, *ACS Catal.*, 2016, **6**, 840–850.

96 J. Ni, Z. Tan, Q. Sai, J. Zhu, X. Wang, B. Lin, J. Lin, C.-t. Au and L. Jiang, Target-oriented confinement of Ru-Co nanoparticles inside N-doped carbon spheres *via* a benzoic acid guided process for high-efficient low-temperature ammonia synthesis, *J. Energy Chem.*, 2021, **57**, 140–146.

97 J. Yang, D. He, W. Chen, W. Zhu, H. Zhang, S. Ren, X. Wang, Q. Yang, Y. Wu and Y. Li, Bimetallic Ru–Co clusters derived from a confined alloying process within zeolite–imidazolate frameworks for efficient NH_3 decomposition and synthesis, *ACS Appl. Mater. Interfaces*, 2017, **9**, 39450–39455.

98 S. Zhang, L. Nguyen, J. X. Liang, J. Shan, J. J. Liu, A. I. Frenkel, A. Patlolla, W. Huang, J. Li and F. F. Tao, Catalysis on singly dispersed bimetallic sites, *Nat. Commun.*, 2015, **6**, 7938.

99 X.-L. Ma, Y. Yang, L.-M. Xu, H. Xiao, W.-Z. Yao and J. Li, Theoretical investigation on hydrogenation of dinitrogen triggered by singly dispersed bimetallic sites, *J. Mater. Chem. A*, 2022, **10**, 6146–6152.

100 X. L. Ma, J. C. Liu, H. Xiao and J. Li, Surface single-cluster catalyst for N_2-to-NH_3 thermal conversion, *J. Am. Chem. Soc.*, 2018, **140**, 46–49.

101 T. Nakao, T. Tada and H. Hosono, Transition metal-doped Ru nanoparticles loaded on metal hydrides for efficient ammonia synthesis from first principles, *J. Phys. Chem. C*, 2020, **124**, 1529–1534.

102 R. Cheng, C. Cui and Z. Luo, Catalysis of dinitrogen activation and reduction by a single Fe_{13} cluster and its doped systems, *Phys. Chem. Chem. Phys.*, 2023, **25**, 1196–1204.

103 R. T. Hannagan, G. Giannakakis, M. Flytzani-Stephanopoulos and E. C. H. Sykes, Single-atom alloy catalysis, *Chem. Rev.*, 2020, **120**, 12044–12088.

104 T. J. Zhang, A. G. Walsh, J. H. Yu and P. Zhang, Single-atom alloy catalysts: structural analysis, electronic properties and catalytic activities, *Chem. Soc. Rev.*, 2021, **50**, 569–588.

105 Y. Zhang, J. Li, J. Cai, L. Yang, T. Zhang, J. Lin, X. Wang, C. Chen, L. Zheng, C.-t. Au, B. Yang and L. Jiang, Construction of spatial effect from atomically dispersed Co anchoring on subnanometer Ru cluster for enhanced N_2-to-NH_3 conversion, *ACS Catal.*, 2021, **11**, 4430–4440.

106 Y. Zhang, X. Peng, J. Deng, F. Sun, J. Cai, Y. Zhou, J. Ni, B. Lin, L. Zheng, X. Wang, J. Lin and L. Jiang, Tuning N_2 activation pathway over Ru/Co sub-nanometer alloy for efficient ammonia synthesis, *J. Catal.*, 2021, **404**, 440–450.

107 A. R. Cholach and A. A. Bryliakova, Re-Co alloys and single-atom Re catalysts in ammonia synthesis: a DFT study, *Mol. Catal.*, 2021, **513**, 111801.

108 Y. Zhang, S. Li, C. Sun, P. Wang, Y. Yang, D. Yi, X. Wang and J. Yao, Understanding and modifying the scaling relations for ammonia synthesis on dilute metal alloys: from single-atom alloys to dimer alloys, *ACS Catal.*, 2022, **12**, 9201–9212.

109 A. R. Singh, J. H. Montoya, B. A. Rohr, C. Tsai, A. Vojvodic and J. K. Norskov, Computational design of active site structures with improved transition-state scaling for ammonia synthesis, *ACS Catal.*, 2018, **8**, 4017–4024.

110 M. Kitano, Y. Inoue, H. Ishikawa, K. Yamagata, T. Nakao, T. Tada, S. Matsuishi, T. Yokoyama, M. Hara and H. Hosono, Essential role of hydride ion in ruthenium-based ammonia synthesis catalysts, *Chem. Sci.*, 2016, **7**, 4036–4043.

111 Y. Zhou, C. Wang, X. Peng, T. Zhang, X. Wang, Y. Jiang, H. Qi, L. Zheng, J. Lin and L. Jiang, Boosting efficient ammonia synthesis over atomically dispersed Co-based catalyst *via* the modulation of geometric and electronic structures, *CCS Chem.*, 2022, **4**, 1758–1769.

112 S. Wu, Y.-K. Peng, T.-Y. Chen, J. Mo, A. Large, I. McPherson, H.-L. Chou, I. Wilkinson, F. Venturini, D. Grinter, P. Ferrer Escorihuela, G. Held and S. C. E. Tsang, Removal of hydrogen poisoning by electrostatically polar MgO support for low-pressure NH_3 synthesis at a high rate over the Ru catalyst, *ACS Catal.*, 2020, **10**, 5614–5622.

113 L. M. Azofra, N. Morlanes, A. Poater, M. K. Samantaray, B. Vidjayacoumar, K. Albahily, L. Cavallo and J. M. Basset, Single-site molybdenum on solid support materials for

catalytic hydrogenation of N$_2$-into-NH$_3$, *Angew. Chem., Int. Ed.*, 2018, **57**, 15812–15816.

114 J. Z. Qiu, J. B. Hu, J. G. Lan, L. F. Wang, G. Y. Fu, R. J. Xiao, B. H. Ge and J. X. Jiang, Pure siliceous zeolite-supported Ru single-atom active sites for ammonia synthesis, *Chem. Mater.*, 2019, **31**, 9413–9421.

115 H. Duan, J.-C. Liu, M. Xu, Y. Zhao, X.-L. Ma, J. Dong, X. Zheng, J. Zheng, C. S. Allen, M. Danaie, Y.-K. Peng, T. Issariyakul, D. Chen, A. I. Kirkland, J.-C. Buffet, J. Li, S. C. E. Tsang and D. O'Hare, Molecular nitrogen promotes catalytic hydrodeoxygenation, *Nat. Catal.*, 2019, **2**, 1078–1087.

116 Y. Zhou, C.-Q. Xu, Z. Tan, H. Cai, X. Wang, J. Li, L. Zheng, C.-t. Au, J. Li and L. Jiang, Integrating dissociative and associative routes for efficient ammonia synthesis over a TiCN-promoted Ru-based catalyst, *ACS Catal.*, 2022, **12**, 2651–2660.

117 L. H. Mou, T. T. Han, P. E. S. Smith, E. Sharman and J. Jiang, Machine learning descriptors for data-driven catalysis study, *Adv. Sci.*, 2023, **10**, 2301020.

118 T. Toyao, Z. Maeno, S. Takakusagi, T. Kamachi, I. Takigawa and K. Shimizu, Machine learning for catalysis informatics: recent applications and prospects, *ACS Catal.*, 2020, **10**, 2260–2297.

119 X.-C. Hu, X.-P. Fu, W.-W. Wang, X. Wang, K. Wu, R. Si, C. Ma, C.-J. Jia and C.-H. Yan, Ceria-supported ruthenium clusters transforming from isolated single atoms for hydrogen production *via* decomposition of ammonia, *Appl. Catal., B*, 2020, **268**, 118424–118437.